New Scalar Measures of Geodetic Strain and Moment Rate from Kinematic Mode Decomposition: Application to the Southwestern United States

Corné Kreemer[1]

[1] Nevada Bureau of Mines and Geology, and Nevada Seismological Laboratory, University of Nevada, Reno

Corresponding author: Corné Kreemer (kreemer@unr.edu)

Key Words:

- Kinematics of crustal and mantle deformation
- Space geodetic surveys
- Dynamics: seismotectonics
- Mechanics, theory, and modelling

****

This is a non-peer reviewed preprint submitted to EarthArXiv. The preprint was submitted to Geophysical Journal International for peer review

****

SUMMARY

Scalar representations of geodetic strain rate tensors are widely used to characterize crustal deformation and, in seismic hazard assessment, to convert strain rate to expected seismic moment rate. Existing scalar definitions of shear strain rate, total strain rate and deformation style are not defined consistently and, because they depend on eigenvalues that carry both dilatation and shear, cannot be read as a partition of mixed-strain deformation. We propose definitions motivated by fault kinematics. The strike-slip strain rate ($\dot{\varepsilon}_s$), derived from the shear on zero-length-change orientations, is twice the geometric mean of the principal strain rate magnitudes and zero when both share a sign. The total strain rate ($\dot{\varepsilon}_t$) is the explicit sum of $\dot{\varepsilon}_s$ and the absolute dilatation ($|\dot{\varepsilon}_d|$); except for uniaxial strain it exceeds the Frobenius norm ($\dot{\varepsilon}_f$), by up to a factor $\sqrt{3}$. The style parameter equals the fractional dilatational contribution in mixed-strain deformation and is extended to classify deformation in which both principal strain rates share a sign. We also propose a moment rate ($\dot{M}_{\text{split}}$) that releases the strike-slip and dilatational contributions on separate strike-slip and dip-slip faults; for Andersonian dips it exceeds the minimum moment ($\dot{M}_{\text{min}}$) by up to 37% for mixed-faulting settings. An application to southwestern U.S. geodetic strain rates shows that the 37% maximum difference is not a corner case: in the 53% of the area where each of the strike-slip and dilatational contributions is at least a quarter of the total strain rate, $\dot{M}_{\text{split}}$ exceeds $\dot{M}_{\text{min}}$ by 34%. The southwestern U.S. example demonstrates that these differences can be regionally significant, with moment-rate estimates differing by tens of percent in mixed-style deformation zones.

1. INTRODUCTION

Strain rate tensors describing horizontal crustal deformation are useful indicators for relating surface kinematics to the driving forces and to the strain released by earthquakes. Mapping infinitesimal strain rate fields has become an active research area in recent years, spurred by the proliferation of GNSS station velocity data (Blewitt et al., 2018) and the development of multiple new estimation approaches (Goudarzi et al., 2015; Haines et al., 2015; Kreemer et al., 2018, 2020; Männel et al., 2026; Masson et al., 2014; Okazaki et al., 2021; Pagani et al., 2021; Sandwell & Wessel, 2016; Shen et al., 2015; Tape et al., 2009).

For mapping purposes, comparison between studies, and seismic hazard applications, strain rate tensor fields are often reduced to scalar measures. The definition of strain rate scalars matters because they set the amount of deformation available for earthquake generation, and are central to the estimation of geodetic moment rate. The latter can be compared to the observed seismic moment release, the moment rate implied by fault slip rates (with implications for off-fault deformation), and the expected rate of earthquake occurrence. Strain rate models have indeed been used to forecast earthquake rates (Bird et al., 2010, 2015; Bird & Kreemer, 2015; Nishimura, 2022; Rhoades et al., 2017; Rong et al., 2016; Wei et al., 2023; Yuliastuti et al., 2026; Zheng et al., 2018). The choice of scalar strain rate measure, and the assumptions about

fault orientations, can lead to ambiguity in the conversion from strain rate to moment rate (e.g., Bird et al., 2010; Neha et al., 2025; Nishimura, 2022; Pancha et al., 2006; Stevens & Avouac, 2021; Wei et al., 2023; Yuliastuti et al., 2026).

Scalar quantities of strain rate — 'total strain rate', 'shear strain rate' and 'deformation style' — are not defined consistently across the literature (see, e.g., Tape et al., 2009). Moreover, existing definitions are not designed to separate the dilatational and strike-slip contributions: they depend on single eigenvalues, or combinations of them, which carry both contributions, so that the total strain rate is not the sum of the two contributions and the style cannot be read as the fractional contribution of each. The two contributions are most strongly combined in transtension and transpression, which we refer to as 'mixed-strain'.

Here, we propose definitions motivated by fault kinematics for: 1) the strike-slip strain rate $\dot{\varepsilon}_s$, derived from the shear resolved on a zero-length-change orientation, and 2) the total strain rate $\dot{\varepsilon}_t = \dot{\varepsilon}_s + |\dot{\varepsilon}_d|$, the explicit sum of shear and the absolute dilatation. We also introduce a new style parameter Φ that describes the relative contribution of the dilatational mode in mixed-strain deformation and classifies the remaining styles. The new $\dot{\varepsilon}_t$ is additive under the specific decomposition used to define it: for a tensor with a zero-length-change orientation, the total strain rate equals the sum of the totals of its strike-slip and dilatational parts (Appendix B), which existing measures do not satisfy. It does not extend to arbitrary sums of tensors.

The same mode separation is carried into a new moment rate definition, $\dot{M}_{\text{split}}$, which assumes that the strike-slip and dilatational contributions are released on separate strike-slip and dip-slip fault populations with Andersonian dips (Section 6). For these assumptions, $\dot{M}_{\text{split}}$ exceeds the minimum moment, $\dot{M}_{\text{min}}$, of Savage and Simpson (1997), the smallest moment of any fault population that accommodates the strain rate tensor, by up to 37% in areas of mixed-faulting deformation.

We distinguish statements at three levels. Mathematical statements concern the tensor: definitions, identities and inequalities. Kinematic statements interpret the tensor through orientations of zero length change, the orientations along which a fault could slip without length change along it. Tectonic statements concern how deformation is accommodated, for example on separate strike-slip and dip-slip fault populations, and are assumptions. Sections 2 to 5 and Appendices A to C are mathematical and kinematic; the tectonic interpretation is in Section 6, Appendix D and Section 7. The new definitions are proposed for a specific purpose, separating the dilatational and strike-slip contributions, and the moment rates derived from them are not tested against observed seismic moment release here. Existing definitions serve other purposes, for example the maximum shear as a measure of shape change and the Frobenius norm as the magnitude of the tensor.

The paper is organized as follows. Section 2 presents existing scalar definitions. Section 3 compares them with the new definitions in five illustrative cases. Section 4 introduces the new definitions, and their formal uncertainties are introduced in Appendix C. Section 5 compares new

and existing definitions as a function of deformation style. Section 6 states the tectonic assumptions, derives $\dot{M}_{\text{split}}$ and compares it with existing moment estimates. Section 7 applies the new framework to southwestern U.S. geodetic strain rates. Sections 8 and 9 contain a brief discussion and conclusion.

2. EXISTING SCALAR MEASURES

The two-dimensional infinitesimal strain rate tensor $\dot{\boldsymbol{\varepsilon}}$ is derived from spatial derivatives of the horizontal velocity field $v=(v_x, v_y)$, where x and y denote east and north coordinates:

$$\dot{\boldsymbol{\varepsilon}}=\begin{pmatrix} \dfrac{\partial v_x}{\partial x} & \dfrac{1}{2}\left(\dfrac{\partial v_x}{\partial y}+\dfrac{\partial v_y}{\partial x}\right) \\ \dfrac{1}{2}\left(\dfrac{\partial v_y}{\partial x}+\dfrac{\partial v_x}{\partial y}\right) & \dfrac{\partial v_y}{\partial y} \end{pmatrix}=\begin{pmatrix} \dot{\varepsilon}_{xx} & \dot{\varepsilon}_{xy} \\ \dot{\varepsilon}_{yx} & \dot{\varepsilon}_{yy} \end{pmatrix} \tag{1}$$

The tensor is symmetric by construction: $\dot{\varepsilon}_{xy}=\dot{\varepsilon}_{yx}$. The principal strain rates (eigenvalues of $\dot{\boldsymbol{\varepsilon}}$) are:

$$\dot{\varepsilon}_1, \dot{\varepsilon}_2=\frac{\dot{\varepsilon}_{xx}+\dot{\varepsilon}_{yy}}{2}\pm\sqrt{\left(\frac{\dot{\varepsilon}_{xx}-\dot{\varepsilon}_{yy}}{2}\right)^2+\dot{\varepsilon}_{xy}^2} \tag{2}$$

with $\dot{\varepsilon}_1 \geq \dot{\varepsilon}_2$. The principal axes are orthogonal, and the direction of the $\dot{\varepsilon}_1$ axis, measured counter-clockwise from east, is:

$$\alpha=\frac{1}{2}\,atan2\left(2\dot{\varepsilon}_{xy}, \dot{\varepsilon}_{xx}-\dot{\varepsilon}_{yy}\right) \tag{3}$$

Note that α is undefined for $\dot{\varepsilon}_{xx}=\dot{\varepsilon}_{yy}$ and $\dot{\varepsilon}_{xy}=0$, when every direction is principal.

The trace of $\dot{\boldsymbol{\varepsilon}}$ equals the dilatation rate:

$$\dot{\varepsilon}_d=tr\left(\dot{\boldsymbol{\varepsilon}}\right)=\dot{\varepsilon}_{xx}+\dot{\varepsilon}_{yy}=\dot{\varepsilon}_1+\dot{\varepsilon}_2 \tag{4}$$

Positive $\dot{\varepsilon}_d$ indicates fractional area increase. This definition is the first invariant of the tensor and is generally not contested, although occasionally it is defined as the tensor equivalent: $\dot{\varepsilon}_d/2$.

The principal strain rates are the sum and difference of the isotropic and deviatoric parts of the tensor: $\dot{\varepsilon}_{1,2}=\left(\dot{\varepsilon}_d \pm \dot{\gamma}\right)/2$, where $\dot{\gamma}=\dot{\varepsilon}_1-\dot{\varepsilon}_2$ is the maximum engineering shear strain rate (Table 1). Each eigenvalue therefore carries half of the dilatation and half of the shear, so any scalar built from a single eigenvalue depends on both (Section 3).

Table 1 summarizes the scalar measures of shear strain rate ($\dot{\varepsilon}_s$), total strain rate ($\dot{\varepsilon}_t$), and deformation style (Φ) used in the geodetic literature, together with the new definitions proposed here. Multiple definitions of total strain rate included in Table 1 have been motivated and used in studies relating geodetic strain rates to seismic moment rates (e.g., Kostrov, 1974; Nishimura, 2022; Pancha et al., 2006; Savage & Simpson, 1997; Wei et al., 2023), see also Table 4. The

Frobenius norm is often used to depict total strain rate, and often called the 'second invariant'. The second principal invariant of a 2-D tensor is actually $\det = \dot{\varepsilon}_1 \dot{\varepsilon}_2$, which is negative when the eigenvalues have opposite sign and zero for uniaxial strain, and therefore does not serve as a measure of magnitude (see also Castro-Perdomo et al. (2025)).

Note that, although all expressions are given in Cartesian coordinates for simplicity, all definitions and implications remain when $\dot{\boldsymbol{\varepsilon}}$ is expressed in spherical coordinates.

3. EXISTING DEFINITIONS IN MIXED STRAIN

Existing definitions of shear and total strain rate are simple functions of the principal strain rates, which do not depend on the coordinate system. They are not designed to separate superimposed dilatational and shear deformation. The two modes involve different tensor components, and the tensor of the combined deformation is their sum, but the principal axes rotate when the modes are combined, so the eigenvalues of the sum are not the sum of the eigenvalues. Any scalar formed from a single eigenvalue, from the difference of the eigenvalues, or from their quadratic sum therefore mixes the two contributions, with the dilatation (the sum of the eigenvalues) as the exception. We compare the definitions with two criteria: whether they isolate the shear on orientations of zero length change (a kinematic criterion, Section 4.1), and whether the total is the sum of its dilatational and shear modes (a mathematical criterion). Whether these are the right criteria depends on the tectonic assumptions of Section 6.

We illustrate both criteria with the cases of Figure 1 and Table 2, for a 100×100 km area. In case *A*, uniaxial extension in the *y*-direction results from a northward velocity of 10 mm/yr on the north edge relative to the fixed south edge ($\dot{\varepsilon}_{yy} = 1\times10^{-7}$ yr^{-1}, all other components zero, such that $\dot{\varepsilon}_1 = 1\times10^{-7}$ yr^{-1} and $\dot{\varepsilon}_2=0$). Henceforth, strain rates are in units of 10^{-7} yr^{-1}. In case *B*, simple shear results from an eastward velocity of 10 mm/yr on the north edge ($\dot{\varepsilon}_{xy} = 0.5$, $\dot{\varepsilon}_{xx} = \dot{\varepsilon}_{yy} = 0$ and $\dot{\varepsilon}_1=0.5$ and $\dot{\varepsilon}_2=-0.5$). In case C, both velocities are imposed simultaneously; because the strain rate tensor is linear in the velocity gradients, the tensor of C is the sum of those of A and B, but its eigenvalues are 1.21 and −0.21 rather than 1.5 and −0.5. Case D has half the extension of C and the same simple shear, and case E is equal biaxial extension ($\dot{\varepsilon}_{xx} = \dot{\varepsilon}_{yy} = 1$).

The existing definitions for shear and total strain rate give very different values for the same tensor (Table 2). By the first criterion above, existing definitions of shear strain rate do not isolate strike-slip deformation. Equations (5) and (6) give the maximum shear, a measure of shape change that depends only on the deviatoric components and not on the trace. It is the largest shear on any plane, reached at 45° to the principal axes, where the strain rate along the plane is $\dot{\varepsilon}_d/2$; it should be zero along a fault that slips without length change, so $\dot{\gamma}$ is not the strike-slip strain rate. In Section 4 we show that $\dot{\gamma}^2$ is the sum of the squares of the dilatation and of the new strike-slip strain rate (8) (Eq. 18). As a result, even though case *A* contains no strike-slip component, (5) and (6) assign it shear strain rates of 1.0 and 0.5. Shear as defined by (7)

vanishes for uniaxial extension, but not when shear is superimposed on dilatation: it is 1.00 for *B* and about 0.41 for C, although the simple shear is the same. The total strain rates (9)–(11) vary less among themselves, but they also depend on whether the dilatation is un- or biaxial: for equal biaxial extension (*E*) they give 1.41, 1.00 and 2.00, although all three give 1.00 for uniaxial extension (*A*).

By the second criterion above, none of the existing shear and total strain rate definitions are additive under the strike-slip/dilatational decomposition considered here: $A + B \neq C$. Shear definitions (5)–(7) for *A* and *B* sum to 2.0, 1.0 and 1.0, but are 1.41, 0.71 and 0.41 for *C*, and equations (9)–(11) for the total strain rate give 1.22, 1.21 and 1.21 for C, whereas the values for *A* and *B* sum to 1.71, 1.50 and 1.50. Note that the explicit sum is always larger than the corresponding value for case *C*. Additivity is not a mathematical requirement, but it is the physical expectation if the two modes are accommodated by independent fault systems (Section 6). The new shear strain rate (8) and total strain rate (12) introduced in Section 4 satisfy it.

Existing measures of deformation style are not designed to express the fractional contribution of each mode, but they are often interpreted that way. For an equal admixture of extension and shear (case *C*), equations (13)–(16) give 0.83, 0.82, 0.71 and 0.78 on their respective ranges (Table 1), and for case *D*, where the dilatational contribution is one third of the total, 0.62, 0.58, 0.45 and 0.54. All definitions agree at the end-members (1 for *A* and 0 for *B*), so the differences arise only in mixed-strain settings, and equation (15) does not distinguish uniaxial (*A*) from equal biaxial (*E*) extension, since both give 1. We therefore present a new definition for style in Section 4.

4.NEW SCALAR DEFINITIONS

4.1 Shear strain rate

We define the shear strain rate $\dot{\varepsilon}_s$ as the shear on a fault along a zero-length-change (ZLC) orientation, an orientation along which there is no length change, and call it the ‘strike-slip strain rate’. A fault whose strike is along a ZLC orientation can accommodate the deformation by slip without length change along it. ZLC orientations are kinematically admissible fault orientations, not necessarily the orientations that faults take (Section 6.2); $\dot{\varepsilon}_s$ is the strike-slip strain rate if the shear is accommodated on faults along them. The concept of deformation localizing along ‘zero-extension lines’ (absent when the principal strain rates share a sign) is long established (Hill, 1952; Roscoe, 1970; Stören & Rice, 1975).

We use the engineering convention, so that $\dot{\varepsilon}_s$ is twice the tensorial shear component on the fault. In Appendix A, we determine the ZLC orientations for a given strain rate tensor and derive $\dot{\varepsilon}_s = 2\sqrt{-\dot{\varepsilon}_1\dot{\varepsilon}_2}$ by resolving the tensor in a frame aligned with a ZLC orientation. Because $\dot{\varepsilon}_1\dot{\varepsilon}_2$ is the determinant of the tensor, $\dot{\varepsilon}_s$ does not depend on the coordinate system (Appendix A.3). Below we show that the same result follows geometrically from the Mohr circle for strain

rate: the circle crosses the shear axis at two planes whose normals are the ZLC orientations, and $\dot{\varepsilon}_s$ is twice the shear coordinate at the crossing (Figure 2).

Each point on the Mohr circle represents strain rates on a unique plane, with a value $\dot{\varepsilon}_{nn}$ normal to a plane and $\dot{\varepsilon}_{tn}$ for the tensorial shear strain rate across the plane. The circle is centered at $\dot{\varepsilon}_d/2$ on the $\dot{\varepsilon}_{nn}$ axis, has a radius $\dot{\gamma}/2=(\dot{\varepsilon}_1-\dot{\varepsilon}_2)/2$ (i.e., the maximum tensor shear strain rate ((6) Table 1)), and crosses the $\dot{\varepsilon}_{nn}$ axis at $\dot{\varepsilon}_1$ and $\dot{\varepsilon}_2$. A plane whose normal makes an angle ϕ with the $\dot{\varepsilon}_1$ axis plots at an angle 2ϕ from the point $\dot{\varepsilon}_1$, with $\dot{\varepsilon}_{nn}=\dot{\varepsilon}_d/2+(\dot{\gamma}/2)\cos 2\phi$ and $\dot{\varepsilon}_{\mathrm{tn}}=(\dot{\gamma}/2)\sin 2\phi$ (Appendix A.4).

The circle crosses the $\dot{\varepsilon}_{tn}$ axis only if the principal strain rates have opposite signs. The two points where it does (the stars in Figure 2) are the planes with no strain rate in the direction of their normal ($\dot{\varepsilon}_{nn}=0$). There is no length change along the normal of a star plane, so that normal is a ZLC orientation, and a fault along it lies perpendicular to the star plane. The two ZLC orientations are conjugate: one is left-lateral (upper star) and one right-lateral (lower star). Half the angle between the $\dot{\varepsilon}_1$ point and a star is ϕ_{ZLC}. The distance from the origin to the center of the circle is $|\dot{\varepsilon}_d|/2$, the radius is $\dot{\gamma}/2$, and the shear coordinate of a star, which we denote $\dot{\varepsilon}_s/2$, completes a right triangle with these two. Pythagoras' theorem gives:

$$\left(\frac{\dot{\varepsilon}_d}{2}\right)^2+\left(\frac{\dot{\varepsilon}_s}{2}\right)^2=\left(\frac{\dot{\gamma}}{2}\right)^2 \;\Rightarrow\; \dot{\varepsilon}_s/2=\pm\sqrt{-\dot{\varepsilon}_1\dot{\varepsilon}_2} \tag{18}$$

The shear strain rate on a ZLC orientation is $\dot{\varepsilon}_s=2\sqrt{-\dot{\varepsilon}_1\dot{\varepsilon}_2}$, twice the tensorial shear, in agreement with Appendix A (Eq. A9). Setting $\dot{\varepsilon_{nn}}=0$ gives $\cos 2\phi_{\mathrm{ZLC}}=-\dot{\varepsilon}_d/\dot{\gamma}$ from which follows $\tan^2\phi_{\mathrm{ZLC}}=-\dot{\varepsilon}_1/\dot{\varepsilon}_2$ (see Appendix A.4), the same orientations as derived algebraically in Appendix A (Eq. A4).

Equation (18) also shows why the maximum shear strain rate $\dot{\gamma}$ (5) is not the strike-slip strain rate: $\dot{\gamma}^2=\dot{\varepsilon}_d^2+\dot{\varepsilon}_s^2$, so $\dot{\gamma}\geq\dot{\varepsilon}_s$, with equality only for zero dilatation (Section 3). For cases *C* and *D*, $\dot{\gamma}=\sqrt{2}$ and $\sqrt{5}/2$, whereas $\dot{\varepsilon}_s=1$ for both (Table 2).

Angle ϕ in a Mohr circle represents the angle to the normal of a plane. A fault along a ZLC orientation is the plane perpendicular to a star, at the diametrically opposite point of the circle, where the strain rate across it is $\dot{\varepsilon}_d$ and the shear is $\pm\dot{\varepsilon}_s/2$. On a ZLC orientation the shear is parallel to the fault and the dilatation acts across it. In the frame of the fault, the tensor has only two non-zero components: the shear $\dot{\varepsilon}_{tn}$ along the fault, and the normal strain rate $\dot{\varepsilon}_d$ across it, which carries the whole areal dilatation rate (Appendix A.2). In the isotropic–deviatoric decomposition, in contrast, the dilatation is shared equally between the two directions ($\dot{\varepsilon}_d/2$ each), and the deviatoric part mixes strike-slip shear and dilatation (Section 3). Section 6 interprets the dilatational part in terms of dip-slip faulting.

For uniaxial strain ($\dot{\varepsilon}_1=0$ or $\dot{\varepsilon}_2=0$) the circle touches the $\dot{\varepsilon}_{tn}$ axis at the origin, the two ZLC orientations coincide and $\dot{\varepsilon}_s=0$, so that only the dilatation remains. When both principal strain rates have the same sign ($\dot{\varepsilon}_1\dot{\varepsilon}_2>0$), the circle does not cross the $\dot{\varepsilon}_{tn}$ axis, confirming geometrically that there are no ZLC orientations, and $\dot{\varepsilon}_s=0$.

4.2 Total strain rate

The total strain rate $\dot{\varepsilon}_t=\dot{\varepsilon}_s+|\dot{\varepsilon}_d|$ is the sum of the strike-slip strain rate and the absolute dilatation strain rate, so that the contributions of the dilatational and strike-slip modes add (Appendix B). In this paper 'total strain rate' refers to $\dot{\varepsilon}_t$, and the other measures in Table 1 are named individually. $\dot{\varepsilon}_t$ does not depend on the coordinate system either, because $\dot{\varepsilon}_s$ and $\dot{\varepsilon}_d$ (i.e., the trace) do not.

The total strain rate is never smaller than the Frobenius norm $\dot{\varepsilon}_f$ (9), the most common existing measure. When $\dot{\varepsilon}_s>0$, $\dot{\varepsilon}_f^2=(\dot{\varepsilon}_d^2+\dot{\gamma}^2)/2=\dot{\varepsilon}_d^2+\dot{\varepsilon}_s^2/2$, using $\dot{\gamma}^2=\dot{\varepsilon}_d^2+\dot{\varepsilon}_s^2$ (Eq. 18), so that

$$\dot{\varepsilon}_t^2-\dot{\varepsilon}_f^2=(|\dot{\varepsilon}_d|+\dot{\varepsilon}_s)^2-\dot{\varepsilon}_d^2-\frac{\dot{\varepsilon}_s^2}{2}=2|\dot{\varepsilon}_d|\dot{\varepsilon}_s+\frac{\dot{\varepsilon}_s^2}{2}\geq 0 \tag{19}$$

When $\dot{\varepsilon}_s=0$, $\dot{\varepsilon}_t^2-\dot{\varepsilon}_f^2=(\dot{\varepsilon}_1+\dot{\varepsilon}_2)^2-\dot{\varepsilon}_1^2-\dot{\varepsilon}_2^2=2\dot{\varepsilon}_1\dot{\varepsilon}_2\geq 0$. Equality therefore holds only for uniaxial strain ($\dot{\varepsilon}_1\dot{\varepsilon}_2=0$). How much smaller $\dot{\varepsilon}_f$ is, as a function of deformation style, is quantified in Section 5.

4.3 Deformation style

The deformation style Φ equals the fractional dilatational contribution ($\Phi=\dot{\varepsilon}_d/\dot{\varepsilon}_t$) for the range $(-1,+1)$. We extend the range to $[-2,+2]$ for the same-sign regime (Table 1): $\Phi=+1+\dot{\varepsilon}_2/\dot{\varepsilon}_1$ when $\dot{\varepsilon}_1\geq\dot{\varepsilon}_2>0$ and $\Phi=-1-|\dot{\varepsilon}_1|/|\dot{\varepsilon}_2|$ when $\dot{\varepsilon}_2\leq\dot{\varepsilon}_1<0$. As a result, $\Phi=0$ for zero dilatation, $|\Phi|=1$ for uniaxial strain rate, and $|\Phi|=2$ for equal biaxial deformation. Most desirably, $\Phi=1/2$ and $\Phi=-1/2$ for equal strike-slip and dilatational contributions, of positive or negative dilatation, respectively.

We refer to the regime in which $\dot{\varepsilon}_1\dot{\varepsilon}_2<0$ ($\dot{\varepsilon}_s>0$, $|\Phi|<1$) as the 'opposite-sign regime', and the regime in which $\dot{\varepsilon}_1\dot{\varepsilon}_2\geq 0$ ($\dot{\varepsilon}_s=0$, $|\Phi|\geq 1$) as the 'same-sign regime'; uniaxial strain, where one principal strain rate is zero, belongs to the latter.

5 COMPARISON BETWEEN NEW AND EXISTING DEFINITIONS

Figure 3 compares the definitions as a function of Φ, normalized such that $\dot{\varepsilon}_t$ is constant across all styles (thus $\dot{\varepsilon}_t$ is the reference, and the ratios quantify how the definitions differ). Figure 3a shows that only the strike-slip strain rate $\dot{\varepsilon}_s$ equals the shear on a zero-length-change orientation in all regimes, by construction. In contrast, the maximum engineering shear strain

rate (5) peaks at 1.0 not only for $\Phi=0$ but also for $|\Phi|=1$, and has a finite value in the same-sign regime: it falls from 1.0 at $\Phi=0$ to a minimum of $1/\sqrt{2}\approx0.71$ at $|\Phi|=1/2$, returns to 1.0 at $|\Phi|=1$, where there is no strike-slip strain rate, and decreases to zero at $|\Phi|=2$ (Table 3). It is therefore non-monotonic and does not by itself indicate the style of deformation, and the same holds for the maximum tensorial shear strain rate (6), which is half as large (not shown in Figure 3a for clarity). The definition of Holt et al. (2000) (7) has a shape similar to (8), but it drops off non-linearly and is always less than $\dot{\varepsilon}_s$ between the end-members, because it is defined by a single eigenvalue (Section 3).

Figure 3b shows that no existing total strain rate definition exceeds $\dot{\varepsilon}_t$. They equal it only for uniaxial strain, where all definitions agree, and, in the case of (11), throughout the same-sign regime, where $\dot{\varepsilon}_t=|\dot{\varepsilon}_d|$. For the Frobenius norm (9) this is proved in Section 4.2, and (10) is never larger than (9). That $\dot{\varepsilon}_t$ is never smaller follows from its linear sum of the strike-slip and dilatational contributions, whereas the Frobenius norm combines them in quadrature (Section 4.2). The difference is largest in the mixed-strain regime, where $\dot{\varepsilon}_f/\dot{\varepsilon}_t$ reaches $1/\sqrt{3}\approx0.58$ ($\dot{\varepsilon}_f$ is 42% smaller than $\dot{\varepsilon}_t$,; $\dot{\varepsilon}_t/\dot{\varepsilon}_f=\sqrt{3}$) at $|\Phi|=1/3$; for zero dilatation and for equal biaxial deformation ($|\Phi|=2$) it is $1/\sqrt{2}\approx0.71$ (29% smaller). Definitions (10) and (11) coincide in the opposite-sign regime, where they are lower than (9) by 0.21 of $\dot{\varepsilon}_t$ at $\Phi=0$ and by 0.04 at $|\Phi|=1/3$, and by less than 0.01 for $|\Phi|>0.49$; in the same-sign regime (10) falls to 0.50 of $\dot{\varepsilon}_t$ at $|\Phi|=2$.

In Figure 3c, the existing style definitions (13), (14), (15) and (16) are plotted relative to the new definition Φ, and all are positive for $0<\Phi<1$ and negative for $-1<\Phi<0$. The largest positive deviations are $+0.33$ for (13) at $\Phi\approx0.5$, $+0.32$ for (14) at $\Phi\approx0.5$, $+0.23$ for (15) at $\Phi\approx0.6$ and $+0.29$ for (16) at $\Phi\approx0.55$ (equal but opposite results for negative Φ), consistent with the equal admixture of Section 3. In the same-sign regime (13) equals Φ, (14) saturates at $\pm\sqrt{2}$, (15) saturates at ±1 and thus does not distinguish uniaxial from biaxial strain, and (16) deviates from Φ by less than 0.1.

Table 3 summarizes the comparison by writing each definition in terms of the dilatation $\dot{\varepsilon}_d$ and, in the opposite-sign regime, the strike-slip strain rate $\dot{\varepsilon}_s$. With the normalization of Figure 3, $\dot{\varepsilon}_d=\Phi$ and $\dot{\varepsilon}_s=1-|\Phi|$, so that the table gives the curves of Figure 3 analytically. Apart from (8), (12) and (17), which are linear or a ratio of linear terms, all definitions combine the two contributions non-linearly, mostly in quadrature (Sections 4.1 and 4.2), so that neither contribution can be recovered from them separately. In the same-sign regime $\dot{\varepsilon}_s=0$, so that $\dot{\varepsilon}_t=|\dot{\varepsilon}_d|$ and $\dot{\varepsilon}_d/\dot{\varepsilon}_t$ would give only $\mathrm{sgn}(\dot{\varepsilon}_d)$, the value of (15); the second variable is therefore Φ as defined in Table 1, determined by the ratio $\dot{\varepsilon}_2/\dot{\varepsilon}_1$. The two columns agree at $|\Phi|=1$.

6. NEW MOMENT RATE DEFINITION

6.1 From strain rate to moment rate

The Kostrov (1974) relation links the moment rate tensor to the strain rate tensor, $\dot{M}_{ij} = 2\mu V \dot{\varepsilon}_{ij}$ where μ is the shear modulus and $V = D A$, with D being the seismogenic thickness and A the area to which the strain rate applies (Appendix D.1). It allows seismic moment tensors to be converted to strain rate tensors, which in some cases are directly compared with geodetic ones (e.g., Castro-Perdomo et al., 2025; Jackson et al., 1994; Jenny et al., 2004; Kreemer et al., 2000; Masson et al., 2005; Middleton et al., 2018; Nucci et al., 2025; Shen-Tu et al., 1995, 1998; Stevens & Avouac, 2021). However, in most studies only scalar quantities are compared, which requires converting the geodetic strain rate tensor to a scalar moment rate. This conversion requires two choices: a scalar measure of the strain rate, and the faulting assumed to accommodate it. Existing conversions differ in both: they use different scalar strain rates (among them (5) and (9) to (11)) and different assumptions about fault orientation. Table 4 gives a summary. Because the strike-slip and dilatational contributions are released on different types of faults, separating them in the strain rate gives a moment rate for each, whereas a scalar strain rate that mixes them cannot be converted to a moment rate without a further assumption about the faulting.

To our knowledge, one study based the conversion on $\dot{\gamma}$ (20) (Working Group on California Earthquake Probabilities, 1995). Stevens and Avouac (2021) combined the Frobenius norm $\dot{\varepsilon}_f$ with a geometric factor $f = 1/(\sin\delta\cos\delta)$ that depends on the fault dip δ (21), and considered the end-members $f = 2$ and $f = 4$ (dips of 45° and 15°). The combination has since been used by Donniol Jouve et al. (2024) and Nucci et al. (2025). The majority of studies have used one of two 'minimum moment' definitions: (22), independently proposed by Ward (1994) and Holt et al. (1995) (the latter in the tensor form (see Table 1)), and (23) proposed by Savage and Simpson (1997) and later also derived by Bird & Liu (2007). (22) and (23) are equal in the opposite-sign regime. In the same-sign regime (23) is larger, because it includes the vertical strain rate, $\dot{\varepsilon}_3 = -\dot{\varepsilon}_d$. This follows from volume conservation: slip in a fault plane causes no volume change (Appendix D.1). (23) is a lower bound for the moment rate of any set of faults that produces the observed horizontal strain rate tensor, and the smallest possible: faults with other orientations, or with slip that partly cancels between faults, need at least as much moment as (23) to produce the same net strain (Appendix D.5). (22) is a looser lower bound. We refer to (23) as $\dot{M}_{\min}$.

6.2 Tectonic assumptions

The new moment rate definition (Section 6.3) rests on four assumptions. They are tectonic, and none of them is implied by the strain rate tensor:

1. The strain is released by faulting (full coupling; Section 8 discusses creep, slow slip and distributed deformation).
2. The strike-slip contribution $\dot{\varepsilon}_s$ is released on strike-slip faults along ZLC orientations (Section 4.1).

3. The dilatational contribution $\dot{\varepsilon}_d$ is released on dip-slip faults of dip δ (normal faults for extension, thrust faults for contraction). Where ZLC orientations exist ($\dot{\varepsilon}_s > 0$), these faults are parallel to the strike-slip faults, so that the dilatation acts across them. In the same-sign regime ($\dot{\varepsilon}_s = 0$) there are no ZLC orientations and no strike-slip term, and any set of dip-slip faults of the same dip and sense that produces the horizontal strain rate tensor gives the same $\dot{M}_{\text{split}} = \dot{M}_{ds}$ (Section 6.3).
4. The two fault populations are separate, and no slip cancels between faults, so that the strain rate amplitudes $\dot{\varepsilon}_s$ and $\dot{\varepsilon}_d$ determine the moment of each population.

The partitioning assumption is supported by observations of slip partitioning in seismic moment release (Célérier, 2008; Frohlich, 2001), including in mixed-strain tectonic environments (e.g., King et al., 2005; Le et al., 2007; Lewis, 2007; Luo & Wang, 2022; Rashidi & Derakhshani, 2022). These observations show that partitioning occurs; they do not show that it holds at every location or for every strain rate tensor.

We use the term “mixed-faulting” for moment release on both strike-slip and dip-slip faults.

6.3 Definition

The strike-slip and dip-slip contributions are:

$$\dot{M}_{ss} = \mu D A \, \dot{\varepsilon}_s, \qquad \dot{M}_{ds} = \mu D A \, f \left| \dot{\varepsilon}_d \right| \tag{25}$$

where f is the dip factor (Section 6.1; Appendix D.2 and D.3). Their sum is the moment rate of the partitioned model:

$$\dot{M}_{\text{split}}(\delta) = \dot{M}_{ss} + \dot{M}_{ds} = \mu D A \left(\dot{\varepsilon}_s + f \left| \dot{\varepsilon}_d \right| \right) \tag{26}$$

We denote the sum in (26) as $\dot{M}_{\text{split}}(\delta)$, the moment rate when the strain is split between strike-slip and dip-slip faults. It is the total moment rate of strike-slip faults on ZLC orientations and dip-slip faults parallel to them (when in the opposite-sign regime), whereas the minimum moment $\dot{M}_{\min}$ is the smallest total that any set of faults can have for the same strain rate, so that $\dot{M}_{\text{split}}$ is never smaller than $\dot{M}_{\min}$, for any dip (Section 6.4).

We consider two sets of dip. For $\delta = 45°$, f is minimized (i.e., $f = 2$) and this case thus serves as one reference. The second case uses the dips preferred by Anderson (1905, 1951) faulting theory, 60° for normal faults and 30° for thrust faults. For the remainder of this paper, $\dot{M}_{\text{split}}$ without an argument denotes the case with Andersonian angles; i.e., $f = 4/\sqrt{3}$. Both $\delta = 45°$ and $\delta = 30°/60°$ are reference cases, not preferred values. Other examples are: $f = 2.0, 2.3, 4.0$ and 5.9 for $\delta = 45°, 30°, 15°$ and $10°$ (Section 6.6).

Bird et al. (2010) replaced the factor of 2 in (23) with $f = 4.46$ (i.e., δ=14°) for subduction zones, and Stevens and Avouac (2021) and Donniol Jouve et al. (2024) include f in (21), in each case applied to the full strain rate tensor. In $\dot{M}_{\text{split}}$ the dip factor applies to the dilatational part only, because only the dip-slip faults are inclined, which makes the dip correction tractable. Stevens and Avouac (2021) also apply a factor to strike-slip faults, for a conjugate set at an assumed angle to the principal axes. The orientation of the strike-slip faults in $\dot{M}_{\text{split}}$ follows from the ZLC condition and the moment from the resolved shear, so no separate factor is applied. Other fault orientations imply other partitions (Section 6.4). Only at zero dilatation are the ZLC orientations the planes of maximum shear.

6.4 Comparison with the minimum moment and Frobenius norm

Figure 4 shows all moment rate definitions in Table 4 as a function of Φ. For any dip δ, $\dot{M}_{\text{split}}(\delta) \geq \dot{M}_{\text{min}}$, because $\dot{M}_{\text{split}}(\delta)$ is the moment rate of a set of faults that produces the observed horizontal strain rate tensor, and $\dot{M}_{\text{min}}$ is the smallest moment rate that any such set can have (Section 6.1). At zero dilatation ($\Phi = 0$), $\dot{\varepsilon}_2 = -\dot{\varepsilon}_1$ and $\dot{\varepsilon}_s = 2\dot{\varepsilon}_1$, so that both moment-rate estimates, (22) and (23), which are lower bounds, become $2\mu D A\ \dot{\varepsilon}_1 = \mu D A\ \dot{\varepsilon}_s$, which is also $\dot{M}_{\text{split}}$ for any dip, because the dip-slip term vanishes. In the same-sign regime, $\dot{M}_{\text{min}} = 2\mu D A |\dot{\varepsilon}_d|$ and $\dot{M}_{\text{split}}(\delta) = \mu D A f |\dot{\varepsilon}_d|$, which are equal for $\delta = 45°$, where $f = 2$: $\dot{M}_{\text{min}}$ then corresponds to dip-slip faults dipping at 45°. In mixed strain ($0 < |\Phi| < 1$), $\dot{M}_{\text{split}}(\delta)$ exceeds $\dot{M}_{\text{min}}$ because of the orientations assumed. $\dot{M}_{\text{min}}$ is itself the moment of a partitioned population: dip-slip faults of 45° dip, striking perpendicular to the principal axis of larger magnitude, take up the dilatation, and strike-slip faults at 45° to the principal axes take up the remaining shear, $2\min(|\dot{\varepsilon}_1|, |\dot{\varepsilon}_2|)$. In $\dot{M}_{\text{split}}$ the dip-slip faults are parallel to the strike-slip faults on ZLC orientations, which leaves the larger strike-slip term $\dot{\varepsilon}_s = 2\sqrt{-\dot{\varepsilon}_1 \dot{\varepsilon}_2}$. For $\delta = 45°$ the excess of $\dot{M}_{\text{split}}(\delta)$ over $\dot{M}_{\text{min}}$ is at most 25%, at $|\Phi| \approx 0.43$. For Andersonian dips the excess is at most 37%, at $|\Phi| \approx 0.48$, and 15% in the same-sign regime, because the dip factor, $4/\sqrt{3}$, exceeds 2.

The Frobenius-based estimate (21) applies the dip factor f to all styles, whereas $\dot{M}_{\text{split}}$ applies it to the dilatational part only. For a fair comparison we set $f = 4/\sqrt{3}$ (Andersonian dips) and call the result $\dot{M}_f = (4/\sqrt{3})\ \mu D A\ \dot{\varepsilon}_f$. The two agree for uniaxial strain. Relative to $\dot{M}_f$, $\dot{M}_{\text{split}}$ is 39% lower for zero dilatation, up to 17% higher in mixed strain (at $|\Phi| \approx 0.54$) and 41% higher for equal biaxial strain. The relatively high $\dot{M}_f$ at zero dilatation arises because of the geometric factor, which is applied to the strike-slip part even though a vertical strike-slip fault has no dip correction (Section 6.3).

6.5 What $\dot{M}_{\text{split}}$ is and is not

Both $\dot{M}_{\text{split}}$ and $\dot{M}_{\text{min}}$ assume that all strain is released by faulting; they differ in the assumed fault populations. Unlike $\dot{M}_{\text{min}}$, which is a lower bound, no upper bound follows from the strain rate tensor, and $\dot{M}_{\text{split}}$ is not one:

- Slip of opposite sense on different faults raises the scalar moment without changing the strain rate tensor.
- Shallower dips raise it: $f = 2.0$, 2.3, 4.0 and 5.9 for $\delta = 45°$, 30°, 15° and 10°.
- Fault populations with other orientations, or with slip that partly cancels between faults, can have a larger moment; the smallest is $\dot{M}_{\min}$ (Section 6.4).

6.6 Equal total strain rate does not imply equal moment rate

For the same $\dot{\varepsilon}_t$, the moment rate of pure dip-slip deformation exceeds that of pure strike-slip deformation by the factor f ($\dot{M}_{ds}$ against $\dot{M}_{ss}$ in Section 6.3). The reason is geometric. A fault dipping at δ accommodates a horizontal extension or contraction through slip along the dip, which exceeds the horizontal displacement by $1/\cos\delta$, and its area exceeds that of a vertical fault of the same depth by $1/\sin\delta$. The same geometric factor is already reflected in the minimum-moment estimate, which $\dot{M}_{\text{split}}(45°)$ reproduces throughout the same-sign regime ($f = 2$).

6.7 Extension to P_{split}

The moment partition extends to potency. Following Kreemer et al. (2024), potency is $P = \dot{\varepsilon}\, T\, A$, with $\dot{\varepsilon}$ a scalar strain rate, T the time and A the area, and the moment is $M = \mu\, D\, P$. With the partitioned strain rate, $P_{\text{split}}(\delta) = P_{ss} + P_{ds}$ with $P_{ss} = \dot{\varepsilon}_s\, T\, A$ and $P_{ds} = f\,|\dot{\varepsilon}_d|\, T\, A$, so that $M_{\text{split}} = \mu\, D\, P_{\text{split}} = \dot{M}_{\text{split}}\, T$.

7. APPLICATION TO THE SOUTHWESTERN U.S.

We apply our new scalar strain rate definitions to the geodetic strain rate model of Kreemer & Young (2022), present maps of $\dot{\varepsilon}_s$, $\dot{\varepsilon}_t$ and Φ, and compare them against $\dot{\gamma}$, $\dot{\varepsilon}_f$ and the style measure (13), respectively (Figure 5). We also compare different moment rate definitions (Table 5 and Figure 6). The Kreemer & Young (2022) model covers the entire western U.S., but we focus on the southwestern U.S., thereby excluding the contractional strain rates that dominate the Pacific Northwest and the very low strain rates in the eastern part of their model. The region we consider (124-111°W and 32.5-42°N) includes the San Andreas fault system, the Eastern California Shear Zone (ECSZ), the Walker Lane, and the Basin and Range. Table 5 shows that strike-slip dominated deformation covers 38% of the area, intermediate styles 53%, near-uniaxial 8%, and near-biaxial 1%.

Shear strain rate definitions $\dot{\varepsilon}_s$ and $\dot{\gamma}$ differ very little (Figure 5), mostly because 1) in the strike-slip dominated areas their definitions are very close, 2) shear strain rates are generally low elsewhere, and 3) there are not many areas with the near-uniaxial and near-biaxial style (9% of total), where $\dot{\varepsilon}_s$ and $\dot{\gamma}$ differ the most (Figure 3).

We show that $\dot{\varepsilon}_t \geq \dot{\varepsilon}_f$ for all styles, with the difference the smallest for areas with near-uniaxial strain rates, of which there are few in the southwestern U.S. Because $\dot{\varepsilon}_t$ is highest along the San Andreas fault system (Figure 5c), the $\dot{\varepsilon}_t - \dot{\varepsilon}_f$ difference is also at a maximum there, with the difference up to 4-5×10^{-7} yr^{-1} near the San Andreas creeping segments (Figure 5d). Elsewhere, the differences are substantial too; e.g., ~2.2×10^{-8} yr^{-1} near Reno, Nevada ($\Phi \approx 0.14$), in the Walker Lane. That value reflects the nearest grid point in the Kreemer & Young model, and is valid for a 17×17 km area.

Maps of the deformation style (Figure 5e-f) appear quite different between the new definition and the one of Kreemer et al. (2014) (13). Many areas that Φ describes as intermediate style fall in the near-uniaxial strain category when using (13) (e.g., large parts of Basin and Range), and some areas that Φ would imply to be dominated by strike-slip are categorized as intermediate by (13) (e.g., parts of the Walker Lane and ECSZ).

Table 5 shows that areas with strike-slip dominated deformation carry 59% of the total $\dot{M}_{\text{split}}$ for the region, whereas areas with intermediate styles account for 34% of the total $\dot{M}_{\text{split}}$. $\dot{M}_{\text{f}}$ places 67% of the regional moment in strike-slip dominated areas and 27% in intermediate styles (62% and 30% for $\dot{M}_{\text{min}}$). $\dot{M}_{\text{f}}$ is so much higher in strike-slip dominated areas than $\dot{M}_{\text{split}}$, because of how $\dot{M}_{\text{f}}$ is defined, with the geometric factor being applied irrespective of style, making it 63% higher than $\dot{M}_{\text{split}}$ in cases of zero dilatation (Figure 4), even though $\dot{\varepsilon}_f$ is actually lower there than $\dot{\varepsilon}_t$.

Overall, $\dot{M}_{\text{split}}$ (incorporating Andersonian dips) is 20% higher than $\dot{M}_{\text{min}}$ and 12% lower than $\dot{M}_{\text{f}}$. When only considering intermediate style areas, $\dot{M}_{\text{split}}$ is 34% higher than $\dot{M}_{\text{min}}$. For $\dot{M}_{\text{split}}$ versus $\dot{M}_{\text{f}}$, the former is 22% lower than the latter in strike-slip dominated areas, which is partly offset with ratios larger than 1.0 in the remainder of the region. In absolute terms, the overall 20% moment rate surplus and 12% deficit correspond to the equivalent of one moment-magnitude (m_{w}) 6.45 earthquake per year (surplus) and one m_{w} 6.38 earthquake per year (deficit). For the conversion to m_{w} we use $(2/3)\log_{10}M - 6.033$, with M in N m (Hanks & Kanamori, 1979), and the conversion assumes all strain is released seismically (Section 8).

Of the overall 20% surplus for $\dot{M}_{\text{split}} - \dot{M}_{\text{min}}$, 51% comes from the intermediate style areas, 43% from the strike-slip dominated areas, and 6% from near-uniaxial and near-biaxial areas. For the 12% overall deficit for $\dot{M}_{\text{split}} - \dot{M}_{\text{f}}$ the strike-slip dominated areas contribute 130% of the net deficit, offset by a ~30% surplus contribution elsewhere. In Figure 6a we grid the m_{w} equivalent for $\dot{M}_{\text{split}}$ applied over a 50-year period (and assuming same D and μ as above). Figure 6b shows the equivalent for $\dot{M}_{\text{split}} - \dot{M}_{\text{min}}$ and Figure 6c-d shows it when $\dot{M}_{\text{split}} - \dot{M}_{\text{f}}$ is positive or negative, respectively. The largest surplus of $\dot{M}_{\text{split}}$ compared to $\dot{M}_{\text{min}}$ occurs near the San Andreas creeping segments, and is equivalent to the moment of an m_{w} 6.1–6.2 earthquake over a 50-year period, although the assumption that all strain is released seismically likely does not apply there. Elsewhere, the fraction of geodetic strain released seismically is largely

unconstrained, but if all is released seismically, the difference between $\dot{M}_{\text{split}}$ and $\dot{M}_{\text{min}}$ accumulated over 50 years corresponds to, e.g., an m_{w} 5.18 earthquake near Reno, Nevada. Compared to $\dot{M}_{\text{f}}$, the smaller $\dot{M}_{\text{split}}$ at the same locale corresponds to an m_{w} 5.30 event per 50 years.

8. DISCUSSION

Presently, a number of definitions exist for scalar values describing various components of the strain rate tensor (Table 1) or the moment rate (Table 4). The definitions differ in what they measure, and the moment rate definitions give estimates that differ by tens of per cent (Table 5). We propose an internally consistent set of definitions that are based on kinematic mode decomposition and that insist that shear strain rate should reflect strike-slip deformation.

The definition of deformation style matters. The following studies used some sort of style measure to infer that 1) strain rates correlate with geothermal potential in areas of transtension (Blewitt et al., 2005; Faulds et al., 2012; Kreemer et al., 2006), 2) the style of the tensor correlates with the observed type of earthquake clustering (Zaliapin & Ben-Zion, 2016), and 3) seismicity's *b*-value is higher when the strain rate tensor indicates extension (Taroni & Carafa, 2023). Because we show how the various definitions vary non-linearly from one another and, more importantly, how our definition can vary substantially from previous ones (up to 0.33, Section 5), studies that based their analysis on the strain rate tensor derived deformation style might benefit from a revisit.

The strain rate tensor alone cannot distinguish partitioned from oblique-slip faulting, or one partition from another. We present $\dot{M}_{\text{split}}$, which is motivated by the explicit kinematic partitioning of the available strain rate onto strike- and dip-slip faults. On the other hand, $\dot{M}_{\text{min}}$ is the moment of a partitioned population with other orientations, and any population, partitioned or oblique, has a moment of at least $\dot{M}_{\text{min}}$ (Section 6.1). The difference between $\dot{M}_{\text{split}}$ and $\dot{M}_{\text{min}}$ measures the sensitivity of the moment rate to the assumed fault orientations, which is most elevated for mixed-strain areas.

The moment rate definitions share a further limitation: each assumes particular fault orientations (the most efficient ones for $\dot{M}_{\text{min}}$; ZLC orientations and Andersonian dips for $\dot{M}_{\text{split}}$). Faults are inherited and can deviate from them. A fault that deviates produces strain rate components that the observed strain rate tensor does not have (for strike-slip faults a shear parallel to the principal axes, for dipping faults a shear in the vertical plane), and other faults must slip to cancel them. The moment released in producing and cancelling these components adds to the total without adding to the net strain rate. For strike-slip and dip-slip faults alike, the moment needed exceeds $\dot{M}_{\text{min}}$ by a factor $1/\cos 2m$, where m is the deviation from the optimal orientation (45° to the principal axes, or a dip of 45°): 15% for $m = 15°$, the Andersonian dips,

and a factor 2 for $m = 30°$. $\dot{M}_{\min}$ is therefore a lower bound, and the orientations of the mapped faults are needed to estimate how much higher the moment rate is.

All new and existing moment rate definitions also still face the intrinsic obstacle that we do not know to what extent the available moment rate is released seismically. Fault creep (or more generally a coupling below 1.0), as well as distributed aseismic deformation, will result in a seismic moment rate less than the geodetic moment rate. The seismic catalogue is, however, too short to confidently infer the long-term seismic moment rate (Frohlich, 2007; McCaffrey, 1997; Ward, 1998; Zaliapin et al., 2005) and it is thus impossible to ascertain whether an observed seismic to geodetic moment rate below 1.0 is significant (Kreemer et al., 2024).

We present standard deviations for the new scalars as a function of the standard deviations in strain rate estimates. However, those uncertainties are likely too low because they do not account for the epistemic uncertainty revealed by the range of model estimates between different models (Maurer & Materna, 2023; Wu et al., 2011).

A comparison between geodetic moment (rate) and seismicity (rate) is statistically more robust than comparison with seismic moment, but still suffers from not knowing what fraction of the strain is released seismically. Therefore, some studies have introduced an empirical correction coefficient reflecting the overall fraction of seismic coupling (Bird et al., 2010; Nishimura, 2022; Wei et al., 2023). This factor is not introduced in Table 4, because the objective here is to compare the definitions.

Which scalar strain rate or moment rate definition is used matters for studies relating the deformation rate to seismicity rate. Both Wei et al. (2023) and Nishimura (2022) found that (20) performs worse than (22) or (23), yet Zeng et al. (2018) used the maximum shear strain rate (5) to argue for a temporal change in the relationship between strain and seismicity rate. Kreemer & Young (2022) and Kreemer et al. (2024) used (22) and found there to be relatively fewer events in the fastest straining areas, whereas Stevens & Avouac (2021) used the Frobenius norm (9) and found there to be relatively more events in the fastest straining areas. These inconsistencies deserve further attention. Comparisons with seismicity rates should use a moment rate rather than a scalar strain rate, because the moment, unlike the scalar, weights the dilatational and strike-slip contributions by the geometry of the faults that accommodate them.

9. CONCLUSIONS

We propose scalar definitions of the strike-slip strain rate $\dot{\varepsilon}_s$ (8), the total strain rate $\dot{\varepsilon}_t$ (12) and the deformation style Φ (17), and a moment rate $\dot{M}_{\text{split}}$ (26) that releases the strike-slip contribution on strike-slip faults and the dilatational contribution on dip-slip faults. Table 6 summarizes which definition answers which question.

The scalar definitions follow from a kinematic decomposition of the horizontal strain rate tensor into shear on a zero-length-change orientation and extension or contraction across it. They depend only on the determinant and the trace of the tensor, and $\dot{\varepsilon}_t$ is the sum of the two contributions. Existing definitions differ from them: the maximum shear strain rate (5) counts dilatation as shear, the Frobenius norm (9) is up to 42% smaller than $\dot{\varepsilon}_t$, and existing style definitions deviate from Φ by up to 0.33 where dilatation and shear both contribute.

$\dot{M}_{\text{split}}$ equals the minimum moment $\dot{M}_{\text{min}}$ (23) at zero dilatation and exceeds it by up to 37% for Andersonian dips in mixed strain. $\dot{M}_{\text{min}}$ is the smallest moment of any fault population that produces the observed tensor; faults that deviate from the optimal orientation by an angle m need $1/\cos 2m$ times as much.

In the southwestern U.S., 53% of the area has a strike-slip and a dilatational contribution that are each at least a quarter of the total strain rate. There $\dot{M}_{\text{split}}$ exceeds $\dot{M}_{\text{min}}$ by 34%, and these areas carry 51% of the regional $\dot{M}_{\text{split}} - \dot{M}_{\text{min}}$ difference. This shows that the choice of definition can change regional moment rates by a fifth. Which choice is closer to the seismic moment release requires a comparison with a seismic moment catalogue of sufficient duration and an estimate of coupling, and the partition itself can be tested with focal mechanisms and mapped fault orientations. Until then, studies should state the definition, the dip, the shear modulus, the seismogenic thickness and the coupling assumed, so that their estimates can be compared.

ACKNOWLEDGEMENTS

All figures are created with Generic Mapping Tools (Wessel et al., 2019). This work is supported by NASA grants 80NSSC22K0463 and 80NSSC25K7895, the National Geospatial-Intelligence Agency, FM, and by the Statewide California Earthquake Center under SCEC Contribution No. 15675.

Figures and Tables

Table 1. New and existing definitions of shear strain rate, total strain rate and deformation style

	Definition	Reference*	Notes
Shear strain rate	$\dot{\varepsilon}_1-\dot{\varepsilon}_2$ (5)	Love (1927); Frank (1966)	Maximum engineering shear strain rate $\dot{\gamma}$, often also written as $\dot{\gamma}_{max}$ [§]
	$(\dot{\varepsilon}_1-\dot{\varepsilon}_2)/2$ (6)	Cauchy (1827); Pope (1966)	Maximum tensor shear strain rate, equivalent to $\sqrt{((\dot{\varepsilon}_{xx}-\dot{\varepsilon}_{yy})/2)^2+\dot{\varepsilon}_{xy}^2}$.
	$2\min(\lvert\dot{\varepsilon}_1\rvert,\lvert\dot{\varepsilon}_2\rvert);\dot{\varepsilon}_1\dot{\varepsilon}_2\leq 0$ $0;\dot{\varepsilon}_1\dot{\varepsilon}_2>0$ (7)	Holt et al. (2000)	Described as "strike-slip component of faulting". Adopted without the factor 2 by Kreemer & Young (2022).
	$\boldsymbol{\dot{\varepsilon}_s=2\sqrt{\max(-\dot{\varepsilon}_1\dot{\varepsilon}_2,0)}}$ (8)	**This study**	Equivalent to $2\sqrt{max(-det(\dot{\boldsymbol{\varepsilon}}),0)}$ with $det(\dot{\boldsymbol{\varepsilon}})=\dot{\varepsilon}_{xx}\dot{\varepsilon}_{yy}-\dot{\varepsilon}_{xy}^2=\dot{\varepsilon}_1\dot{\varepsilon}_2$.
Total strain rate	$\sqrt{\dot{\varepsilon}_1^2+\dot{\varepsilon}_2^2}$ [§§] (9)	Kreemer et al. (2002; 2003)	This is the Frobenius norm ($\sqrt{\mathrm{tr}(\dot{\boldsymbol{\varepsilon}}^T\dot{\boldsymbol{\varepsilon}})}$) and also equals $\sqrt{\dot{\varepsilon}_{xx}^2+\dot{\varepsilon}_{yy}^2+2\dot{\varepsilon}_{xy}^2}$ and, while often called the "second invariant", it is different from the general 2D definition of second invariant (i.e., $\det(\dot{\boldsymbol{\varepsilon}})$). To avoid ambiguity we call (9) $\dot{\varepsilon}_f$.
	$\max(\lvert\dot{\varepsilon}_1\rvert,\lvert\dot{\varepsilon}_2\rvert)$ (10)	Holt et al. (1995); Ward (1994)	Unlike (11), (10) does not assume that 3D volume is conserved.
	$\max(\lvert\dot{\varepsilon}_1\rvert,\lvert\dot{\varepsilon}_2\rvert,\lvert\dot{\varepsilon}_d\rvert)$ (11)	Savage & Simpson (1997); Bird & Liu (2007)	Is generally equal to (10) except when both eigenvalues have same sign, then (11) is larger and equals $\lvert\dot{\varepsilon}_d\rvert$
	$\boldsymbol{\dot{\varepsilon}_t=\dot{\varepsilon}_s+\lvert\dot{\varepsilon}_d\rvert}$ (12)	**This study**	
Deformation style	$\dot{\varepsilon}_d/\max(\lvert\dot{\varepsilon}_1\rvert,\lvert\dot{\varepsilon}_2\rvert)$ (13)	Kreemer et al. (2014)	Range [-2,+2]
	$\dot{\varepsilon}_d/\dot{\varepsilon}_f$ (14)	(Hirschberg & Sutherland, 2024)	Range $[-\sqrt{2},+\sqrt{2}]$. Based on stress analogue of Klein et al. (2009)
	$\dot{\varepsilon}_d/(\lvert\dot{\varepsilon}_1\rvert+\lvert\dot{\varepsilon}_2\rvert)$ (15)	Maurer et al. (2023)	Range [-1,+1]. Takes the same value for uni- and biaxial strain. Johnson (2024) assumed opposite sign.
	$\frac{3}{4}+\frac{1}{\pi}\tan^{-1}(\dot{\varepsilon}_2/\dot{\varepsilon}_1)$ [§§§] (16)	Métois et al. (2025)	Range [0,+1] when $\tan^{-1}$ is evaluated with atan2 (0 for biaxial compression, +1 for biaxial extension).
	$\boldsymbol{\Phi=\dot{\varepsilon}_d/\dot{\varepsilon}_t\ ;\ \dot{\varepsilon}_1\dot{\varepsilon}_2\leq 0}$ (17) $\boldsymbol{\Phi=+1+\dot{\varepsilon}_2/\dot{\varepsilon}_1\ ;\ \dot{\varepsilon}_1\geq\dot{\varepsilon}_2>0}$ $\boldsymbol{\Phi=-1-\lvert\dot{\varepsilon}_1\rvert/\lvert\dot{\varepsilon}_2\rvert\ ;\ \dot{\varepsilon}_2\leq\dot{\varepsilon}_1<0}$	**This Study**	Range [-2,+2]. In terms of eigenvalues: $\Phi=\frac{\dot{\varepsilon}_1+\dot{\varepsilon}_2}{\lvert\dot{\varepsilon}_1+\dot{\varepsilon}_2\rvert+2\sqrt{-\dot{\varepsilon}_1\dot{\varepsilon}_2}}$; $\dot{\varepsilon}_1\dot{\varepsilon}_2\leq 0$

* We focus on the first study/studies that introduced or popularized the definition.

[§] This is sometimes chosen as strain rate scalar in strain-to-moment rate conversions (see table 4, section 6). Also, note that the definition of Frank (1966) was made for finite strain.

[§§] Note that some studies have used a scaled version ($\sqrt{\dot{\varepsilon}_1^2+\dot{\varepsilon}_2^2}/\sqrt{2}$) (Bos et al., 2003; Calais et al., 2006; England & Molnar, 2005; Hatem et al., 2026; Li et al., 2017), which equals the "effective" strain rate as defined in viscous flow theory (Ranalli, 1995), and we will not consider here.

[§§§] This definition goes back to Houseman & England (1986) and Gordon & Houseman (2015). Also note that $\tan^{-1}(\dot{\varepsilon}_2/\dot{\varepsilon}_1)$ was considered by Middleton et al. (2018) as an indicator of the style of faulting.

561 **Table 2.** Values for new and existing definitions of strain rate scalars* for
562 cases shown in Figure 1.

		A	B	C	D	E
	$\dot{\boldsymbol{\varepsilon}}$	$\begin{pmatrix} 0 & 0 \\ 0 & 1 \end{pmatrix}$	$\begin{pmatrix} 0 & 0.5 \\ 0.5 & 0 \end{pmatrix}$	$\begin{pmatrix} 0 & 0.5 \\ 0.5 & 1 \end{pmatrix}$	$\begin{pmatrix} 0 & 0.5 \\ 0.5 & 0.5 \end{pmatrix}$	$\begin{pmatrix} 1 & 0 \\ 0 & 1 \end{pmatrix}$
	$\dot{\varepsilon}_1$ (2)	1	1/2	~1.207	~0.809	1
	$\dot{\varepsilon}_2$ (2)	0	-1/2	~-0.207	~-0.309	1
	α (3)	90°	45°	67.5°	~58.3°	—
	$\dot{\varepsilon}_d$ (4)	1	0	1	1/2	2
Shear strain rate	(5)	1	1	$\sqrt{2}$	$\sqrt{5}/2$	0
	(6)	1/2	1/2	$\sqrt{2}/2$	$\sqrt{5}/4$	0
	(7)	0	1	$\sqrt{2}-1$	$(\sqrt{5}-1)/2$	0
	(8)	**0**	**1**	**1**	**1**	**0**
Total strain rate	(9)	1	$\sqrt{2}/2$	$\sqrt{3/2}$	$\sqrt{3}/2$	$\sqrt{2}$
	(10)	1	1/2	$(1+\sqrt{2})/2$	$(1+\sqrt{5})/4$	1
	(11)	1	1/2	~1.207	$(1+\sqrt{5})/4$	2
	(12)	**1**	**1**	**2**	3/2	**2**
Deformation style	(13)	1	0	$2\sqrt{2}-2$	$(\sqrt{5}-1)/2$	2
	(14)	1	0	$\sqrt{6}/3$	$\sqrt{3}/3$	$\sqrt{2}$
	(15)	1	0	$\sqrt{2}/2$	$\sqrt{5}/5$	1
	(16)§	1	0	~0.784	~0.535	2
	(17)	**1**	**0**	1/2	1/3	**2**

563 * Strain rate units in 1×10^{-7} yr^{-1}

564 § Rescaled from (16) (i.e., 4*(16) -2) to fit [-2,+2] range

Table 3. Definitions of shear strain rate, total strain rate and deformation style expressed in terms of the dilatation $\dot{\varepsilon}_d$ and, in the opposite-sign regime ($\dot{\varepsilon}_s>0$), the strike-slip strain rate $\dot{\varepsilon}_s$. In the same-sign regime ($\dot{\varepsilon}_s=0$), where $\dot{\varepsilon}_d/\dot{\varepsilon}_t=\mathrm{sgn}(\dot{\varepsilon}_d)$, they are expressed in terms of $\dot{\varepsilon}_d$ and Φ as defined in Table 1 (i.e., the extension to $[-2,+2]$), so that $\dot{\varepsilon}_1=\dot{\varepsilon}_d/|\Phi|$ and $\dot{\varepsilon}_2=\dot{\varepsilon}_d(|\Phi|-1)/|\Phi|$ for extension (the magnitudes of $\dot{\varepsilon}_1$ and $\dot{\varepsilon}_2$ are interchanged for contraction). The two columns agree at $|\Phi|=1$. Numbers refer to Table 1.

Definition	In terms of $\dot{\varepsilon}_d$ and $\dot{\varepsilon}_s$ (*for* $\dot{\varepsilon}_s>0$)	In terms of $\dot{\varepsilon}_d$ and Φ (*for* $\dot{\varepsilon}_s=0$)
(5)	$\sqrt{\dot{\varepsilon}_d^2+\dot{\varepsilon}_s^2}$	$\lvert\dot{\varepsilon}_d\rvert\,(2-\lvert\Phi\rvert)/\lvert\Phi\rvert$
(6)	$\frac{1}{2}\sqrt{\dot{\varepsilon}_d^2+\dot{\varepsilon}_s^2}$	$\lvert\dot{\varepsilon}_d\rvert\,(2-\lvert\Phi\rvert)/(2\lvert\Phi\rvert)$
(7)	$\sqrt{\dot{\varepsilon}_d^2+\dot{\varepsilon}_s^2}-\lvert\dot{\varepsilon}_d\rvert$	0
(8)	$\dot{\varepsilon}_s$	0
(9)	$\sqrt{\dot{\varepsilon}_d^2+\dot{\varepsilon}_s^2/2}$	$\lvert\dot{\varepsilon}_d\rvert\sqrt{1+(\lvert\Phi\rvert-1)^2}/\lvert\Phi\rvert$
(10)	$\frac{1}{2}\left(\sqrt{\dot{\varepsilon}_d^2+\dot{\varepsilon}_s^2}+\lvert\dot{\varepsilon}_d\rvert\right)$	$\lvert\dot{\varepsilon}_d\rvert/\lvert\Phi\rvert$
(11)	$\frac{1}{2}\left(\sqrt{\dot{\varepsilon}_d^2+\dot{\varepsilon}_s^2}+\lvert\dot{\varepsilon}_d\rvert\right)$	$\lvert\dot{\varepsilon}_d\rvert$
(12)	$\dot{\varepsilon}_s+\lvert\dot{\varepsilon}_d\rvert$	$\lvert\dot{\varepsilon}_d\rvert$
(13)	$2\dot{\varepsilon}_d/\left(\sqrt{\dot{\varepsilon}_d^2+\dot{\varepsilon}_s^2}+\lvert\dot{\varepsilon}_d\rvert\right)$	Φ
(14)	$\dot{\varepsilon}_d/\sqrt{\dot{\varepsilon}_d^2+\dot{\varepsilon}_s^2/2}$	$\mathrm{sgn}(\dot{\varepsilon}_d)\lvert\Phi\rvert/\sqrt{1+(\lvert\Phi\rvert-1)^2}$
(15)	$\dot{\varepsilon}_d/\sqrt{\dot{\varepsilon}_d^2+\dot{\varepsilon}_s^2}$	$\mathrm{sgn}(\dot{\varepsilon}_d)$
(16) [§]	$1+(4/\pi)\,\mathrm{atan2}(\dot{\varepsilon}_d-\sqrt{\dot{\varepsilon}_d^2+\dot{\varepsilon}_s^2},\dot{\varepsilon}_d+\sqrt{\dot{\varepsilon}_d^2+\dot{\varepsilon}_s^2})$	$\mathrm{sgn}(\dot{\varepsilon}_d)\left[1+(4/\pi)\,\tan^{-1}(\lvert\Phi\rvert-1)\right]$
(17)	$\dot{\varepsilon}_d/(\dot{\varepsilon}_s+\lvert\dot{\varepsilon}_d\rvert)$	Φ [§§]

[§] rescaled (Table 2)

[§§] By definition (see Table 1)

573 **Table 4.** Definitions for the conversion of strain rate to moment rate in terms of the principal
574 strain rates, of $\dot{\varepsilon}_d$ and $\dot{\varepsilon}_s$ (opposite-sign regime, $\dot{\varepsilon}_s > 0$) and of $\dot{\varepsilon}_d$ and Φ (same-sign regime, $\dot{\varepsilon}_s = 0$).
575 All definitions are to be multiplied by μV, with shear modulus μ and volume $V = D A$.

	In terms of $\dot{\varepsilon}_1$ and $\dot{\varepsilon}_2$	**In terms of $\dot{\varepsilon}_d$ and $\dot{\varepsilon}_s$ (*for* $\dot{\varepsilon}_s > 0$)**	**In terms of $\dot{\varepsilon}_d$ and Φ (*for* $\dot{\varepsilon}_s = 0$)**
(20) based on (5)	$2(\dot{\varepsilon}_1 - \dot{\varepsilon}_2)$	$2\sqrt{\dot{\varepsilon}_d^2 + \dot{\varepsilon}_s^2}$	$2\lvert\dot{\varepsilon}_d\rvert\,(2 - \lvert\Phi\rvert)/\lvert\Phi\rvert$
(21) based on (9)	$f\sqrt{\dot{\varepsilon}_1^2 + \dot{\varepsilon}_2^2}$	$f\sqrt{\dot{\varepsilon}_d^2 + \dot{\varepsilon}_s^2/2}$	$f\lvert\dot{\varepsilon}_d\rvert\sqrt{1 + (\lvert\Phi\rvert - 1)^2}/\lvert\Phi\rvert$
(22) based on (10)	$2\max(\lvert\dot{\varepsilon}_1\rvert, \lvert\dot{\varepsilon}_2\rvert)$	$\sqrt{\dot{\varepsilon}_d^2 + \dot{\varepsilon}_s^2} + \lvert\dot{\varepsilon}_d\rvert$	$2\lvert\dot{\varepsilon}_d\rvert/\lvert\Phi\rvert$
(23) based on (11)	$2\max(\lvert\dot{\varepsilon}_1\rvert, \lvert\dot{\varepsilon}_2\rvert, \lvert\dot{\varepsilon}_1 + \dot{\varepsilon}_2\rvert)$	$\sqrt{\dot{\varepsilon}_d^2 + \dot{\varepsilon}_s^2} + \lvert\dot{\varepsilon}_d\rvert$	$2\lvert\dot{\varepsilon}_d\rvert$
(24) $\dot{M}_{\text{split}}$ (this study)	$\mathbf{2\sqrt{\max(-\dot{\varepsilon}_1\dot{\varepsilon}_2, 0)} + f\lvert\dot{\varepsilon}_1 + \dot{\varepsilon}_2\rvert}$	$\dot{\varepsilon}_s + f\lvert\dot{\varepsilon}_d\rvert$	$f\lvert\dot{\varepsilon}_d\rvert$

576 f is the dip factor (Section 6.1) and δ is the fault dip. Bird et al. (2010) replace the factor 2 in (23) by f
577 for subduction zones.

578 **Table 5.** Breakdown of moment rates, moment ratios, and moment differences as a function of
579 deformation style for the southwestern U.S. Except for the ratios, values are shown as
580 percentages of the same quantity for the entire region. Italic rows are parts of the row above and
581 are not included in the total. In the last row, values in parentheses are total differences as
582 percentages of $\dot{M}_{\min}$ and $\dot{M}_{\mathrm{f}}$, respectively. Cells with $|\Phi| \geq 1.75$ (0.03% of the area) are not
583 included.

Style group[§]	area	$\dot{M}_{\mathrm{split}}$	$\dot{M}_{\min}$	$\dot{M}_{f}$	$\dot{M}_{\mathrm{split}}/\dot{M}_{\min}$	$\dot{M}_{\mathrm{split}}/\dot{M}_{\mathrm{f}}$	$\dot{M}_{\mathrm{split}}-\dot{M}_{\min}$	$\dot{M}_{\mathrm{split}}-\dot{M}_{\mathrm{f}}$
Strike-slip dominated	38.5	58.9	62.1	67.0	1.14	0.78	42.8	129.5
Intermediate	52.6	33.9	30.5	27.3	1.34	1.10	51.2	−23.2
contractional	*10.1*	*14.9*	*13.4*	*12.0*	*1.34*	*1.10*	*22.6*	*−10.1*
extensional	*42.5*	*19.0*	*17.1*	*15.3*	*1.34*	*1.10*	*28.6*	*−13.1*
Near-uniaxial	7.7	5.8	6.0	4.7	1.17	1.09	4.9	−3.7
contractional	*1.4*	*3.5*	*3.6*	*2.8*	*1.16*	*1.10*	*2.9*	*−2.4*
extensional	*6.3*	*2.3*	*2.3*	*1.9*	*1.17*	*1.08*	*2.0*	*−1.3*
Near-biaxial	1.2	1.4	1.5	1.0	1.15	1.28	1.1	−2.5
contractional	*1.1*	*1.1*	*1.2*	*0.8*	*1.15*	*1.31*	*0.9*	*−2.1*
extensional	*0.1*	*0.3*	*0.3*	*0.2*	*1.15*	*1.24*	*0.2*	*−0.4*
Region total	**100**	**100**	**100**	**100**	**1.20**	**0.88**	**100 (+20%)**	**100 (−12%)**

584 [§] Strike-slip dominated is defined as $-0.25 \leq \Phi < 0.25$, Intermediate is the combination of
585 contractional ($-0.75 \leq \Phi < -0.25$) and extensional ($0.25 \leq \Phi < 0.75$) areas, Near-uniaxial is the
586 combination of contractional ($-1.25 \leq \Phi <$ -0.75) and extensional ($0.75 \leq \Phi < 1.25$) areas, and
587 Near-biaxial is the combination of contractional ($-1.75 \leq \Phi <$ -1.25) and extensional (
588 $1.25 \leq \Phi < 1.75$) areas. Combined rows are computed from the pooled areas and moments, so
589 their ratios are ratios of the pooled moments, not averages of the ratios.

590 **Table 6.** The definitions of this study and the question each one answers

	Question	Definition	Note
Strain Rate	How much is the strike-slip deformation?	$\dot{\varepsilon}_s$ (8)	The shear on zero-length-change orientations. The maximum shear (5) exceeds it by 41% at $\Phi = 0.5$ and by a factor 3 at 0.75. In the same-sign regime $\dot{\varepsilon}_s = 0$ is a convention.
	What is the total deformation rate?	$\dot{\varepsilon}_t$ (12)	The sum of the strike-slip and dilatational contributions. The Frobenius norm (9) is up to 42% smaller.
	What is the mix of dilatation and shear?	Φ (17)	Linear in the dilatational fraction; separates uniaxial from equal biaxial strain.
Moment Rate	What is the smallest geodetic moment rate?	$\dot{M}_{\min}$ (23)	A lower bound for any fault population (Appendix D.5).
	What is the moment rate for a stated faulting model?	$\dot{M}_{\text{split}}(\delta)$ (26)	An explicit partition; the assumptions are in Section 6.2.

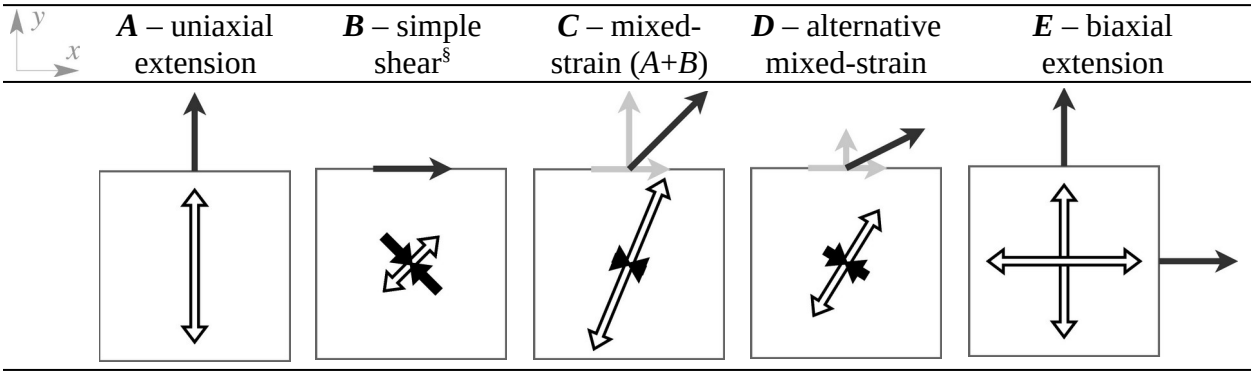


Figure 1. Graphic display of two end-member cases (*A* = uniaxial extension, *B* = simple shear§), mixed-strain (*C*=*A*+*B*), alternative mixed-strain (*D*), and biaxial extension (*E*). Strain rates are reported in Table 2 and are based on *dx*,*dy*=100 km and $v_{x,y}$ = 10 mm/yr, except v_y = 5 mm/yr for case *D*. Thin black and grey vectors are velocity boundary conditions and thick vectors inside square indicate the principal strain rate directions and relative magnitudes, with positive values (extension) in white and negative values (contraction) in black. § Case *B* is simple shear by construction, but its strain rate tensor is identical to that of pure shear.

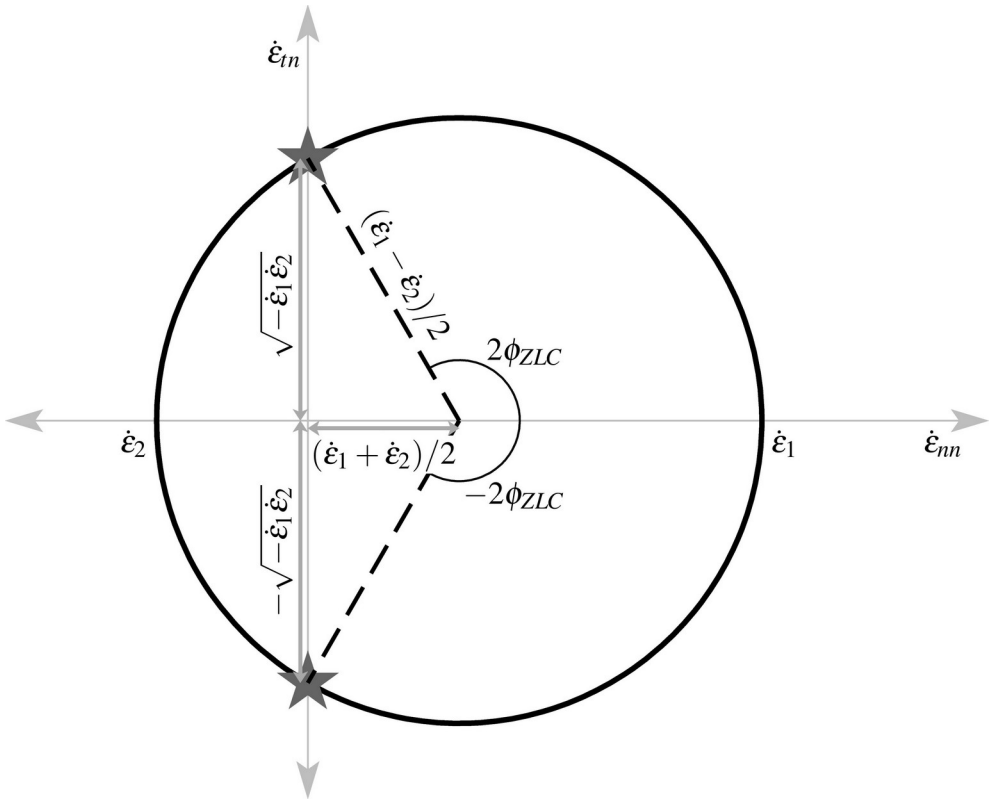
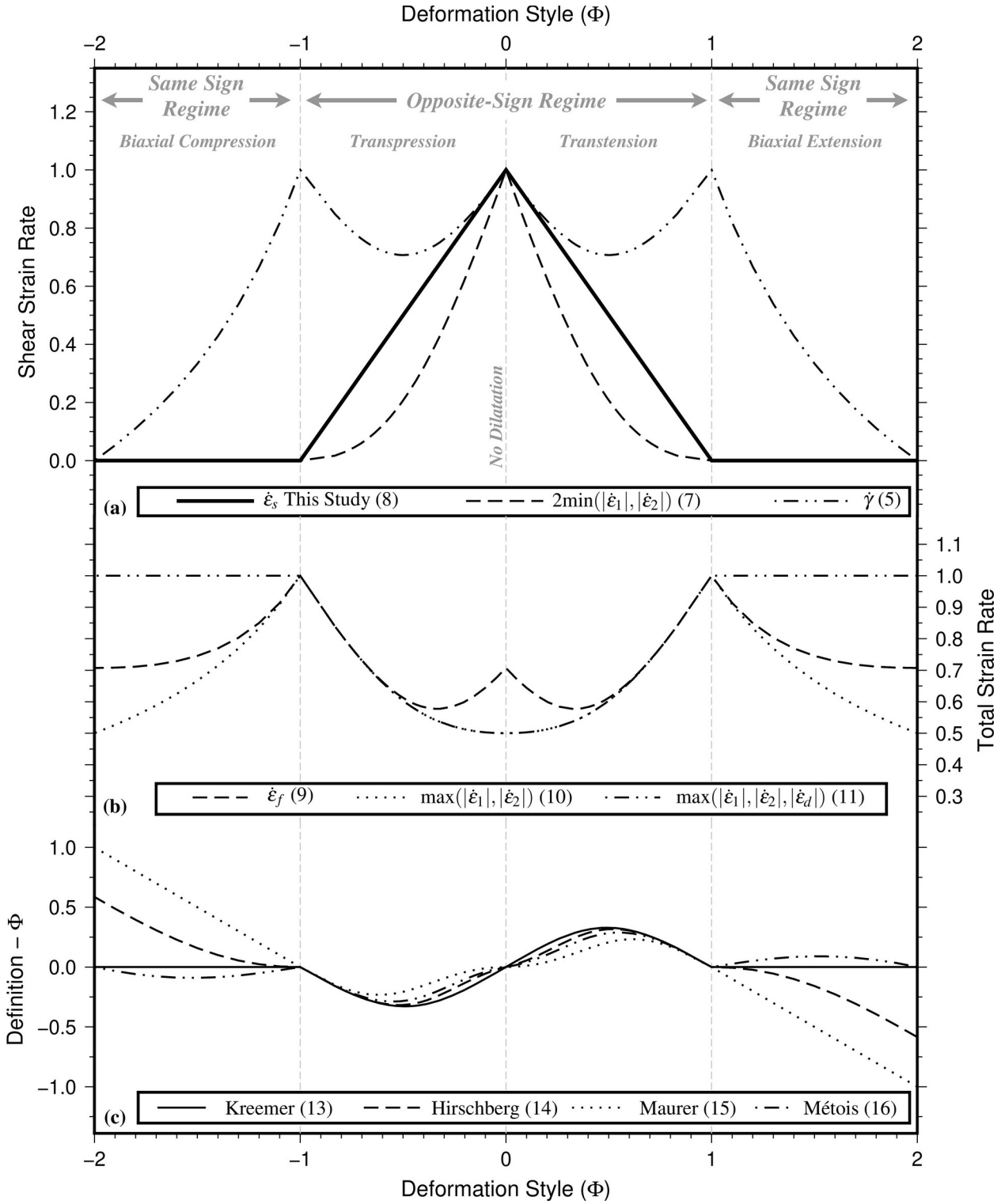


Figure 2. Mohr circle for strain rate (here $\dot{\varepsilon}_1 : \dot{\varepsilon}_2 = 3 : -1$), showing the strain rate normal to a plane ($\dot{\varepsilon}_{nn}$) and the tensorial shear strain rate across a plane ($\dot{\varepsilon}_{tn}$). A point at angle 2ϕ from the $\dot{\varepsilon}_1$ point (both counter-clockwise) is the plane whose normal makes angle ϕ with the $\dot{\varepsilon}_1$ axis. The two stars ($\dot{\varepsilon}_{nn}=0$) have normals along the two zero-length-change (ZLC) orientations, at $\phi=\pm\phi_{ZLC}$ from the $\dot{\varepsilon}_1$ axis. The ZLC orientation is left-lateral ($\alpha + \phi_{ZLC}$) for the upper star and right-lateral ($\alpha - \phi_{ZLC}$) for the lower. Geographically, $\theta_{ZLC} = \alpha \pm \phi_{ZLC}$, counter-clockwise from east, where α is the angle of the $\dot{\varepsilon}_1$ axis.



605 **Figure 3.** Definitions of (a) shear strain rate, (b) total strain rate and (c) deformation style as a
606 function of the deformation style Φ, for $\dot{\varepsilon}_t = 1$ (all values in (a) and (b) are relative to $\dot{\varepsilon}_t$). In (c),
607 each definition is shown relative to Φ, the value of this study (17). In (b), (10) and (11) coincide
608 in the opposite-sign regime.

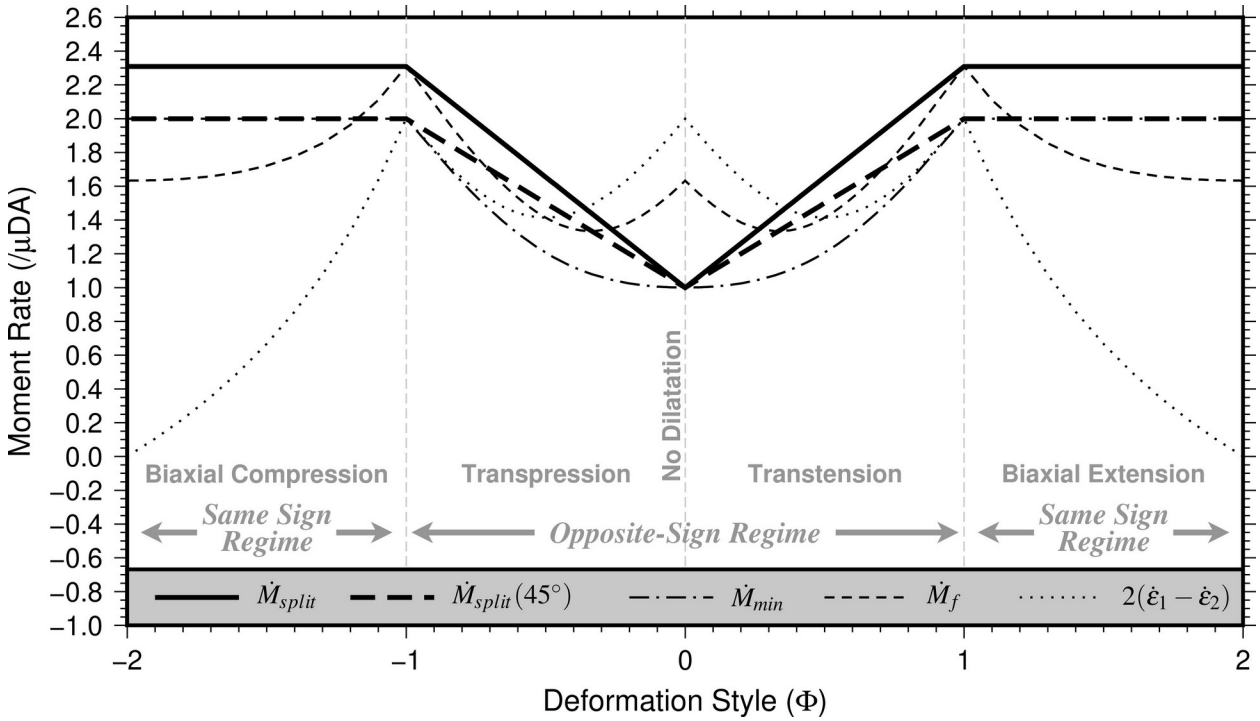


Figure 4. Different moment rate definitions as a function of deformation style Φ. Eigenvalues are normalized by $\dot{\varepsilon}_t$. The curve based on the Frobenius norm (21) is $\dot{M}_f$: it assumes $f = 4/\sqrt{3}$ (Andersonian dips, 30° and 60°) for all styles.

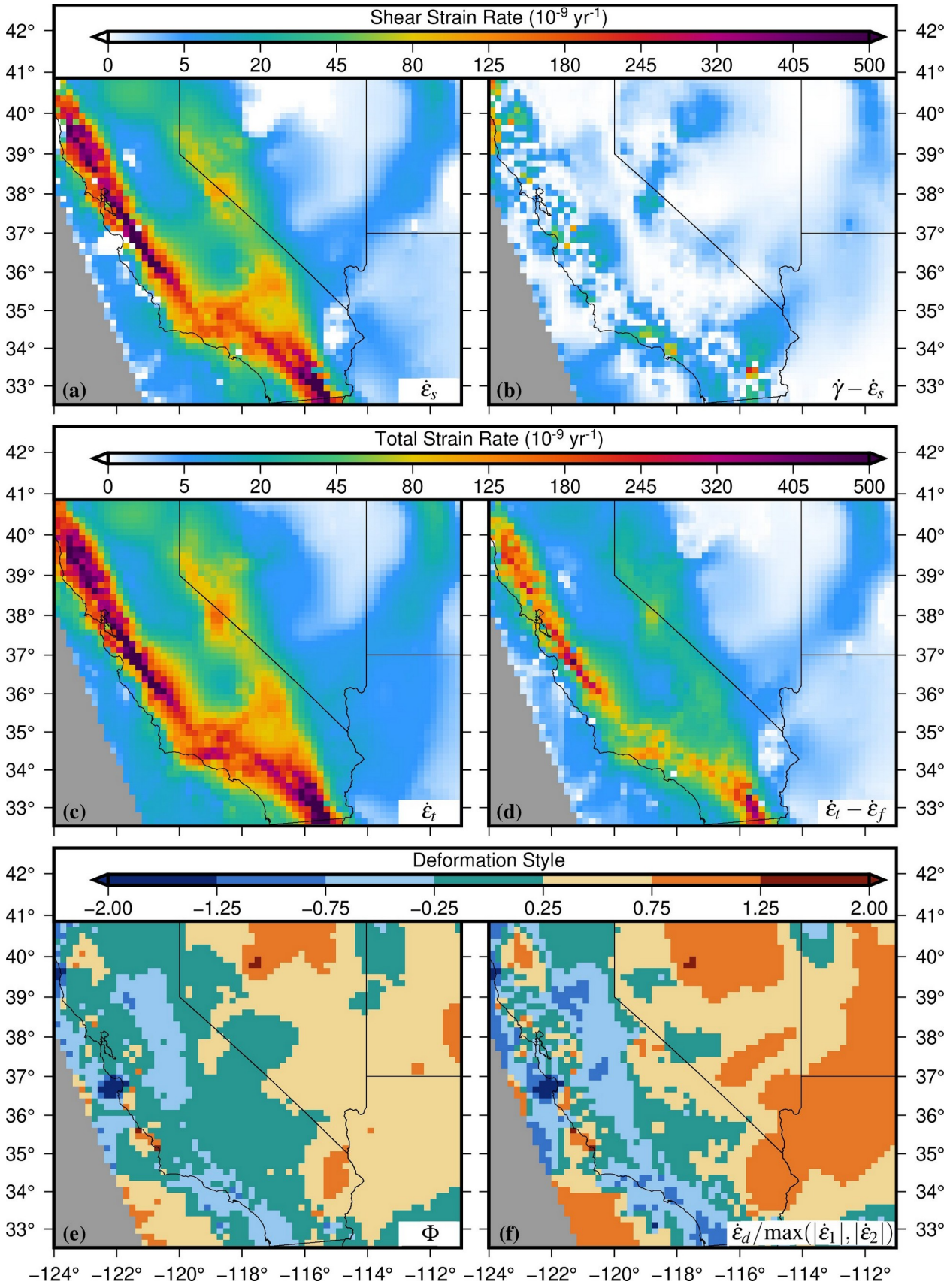

Shear Strain Rate (10^{-9} yr^{-1})
0 5 20 45 80 125 180 245 320 405 500
(a) $\dot{\varepsilon}_s$
(b) $\dot{\gamma} - \dot{\varepsilon}_s$
Total Strain Rate (10^{-9} yr^{-1})
0 5 20 45 80 125 180 245 320 405 500
(c) $\dot{\varepsilon}_t$
(d) $\dot{\varepsilon}_t - \dot{\varepsilon}_f$
Deformation Style
−2.00 −1.25 −0.75 −0.25 0.25 0.75 1.25 2.00
(e) Φ
(f) $\dot{\varepsilon}_d / \max(|\dot{\varepsilon}_1|, |\dot{\varepsilon}_2|)$
42° 41° 40° 39° 38° 37° 36° 35° 34° 33°
−124° −122° −120° −118° −116° −114° −112°

Figure 5. Geodetic strain rate model of Kreemer & Young (2022) expressed as (a) $\dot{\varepsilon}_s$ (8), (b) $\dot{\gamma}$ (5) minus $\dot{\varepsilon}_s$, (c) $\dot{\varepsilon}_t$ (12), (d) $\dot{\varepsilon}_t$ - $\dot{\varepsilon}_f$ (9), (e) Φ (17), (f) $\dot{\varepsilon}_d / max(|\dot{\varepsilon}_1|, |\dot{\varepsilon}_2|)$ (13).

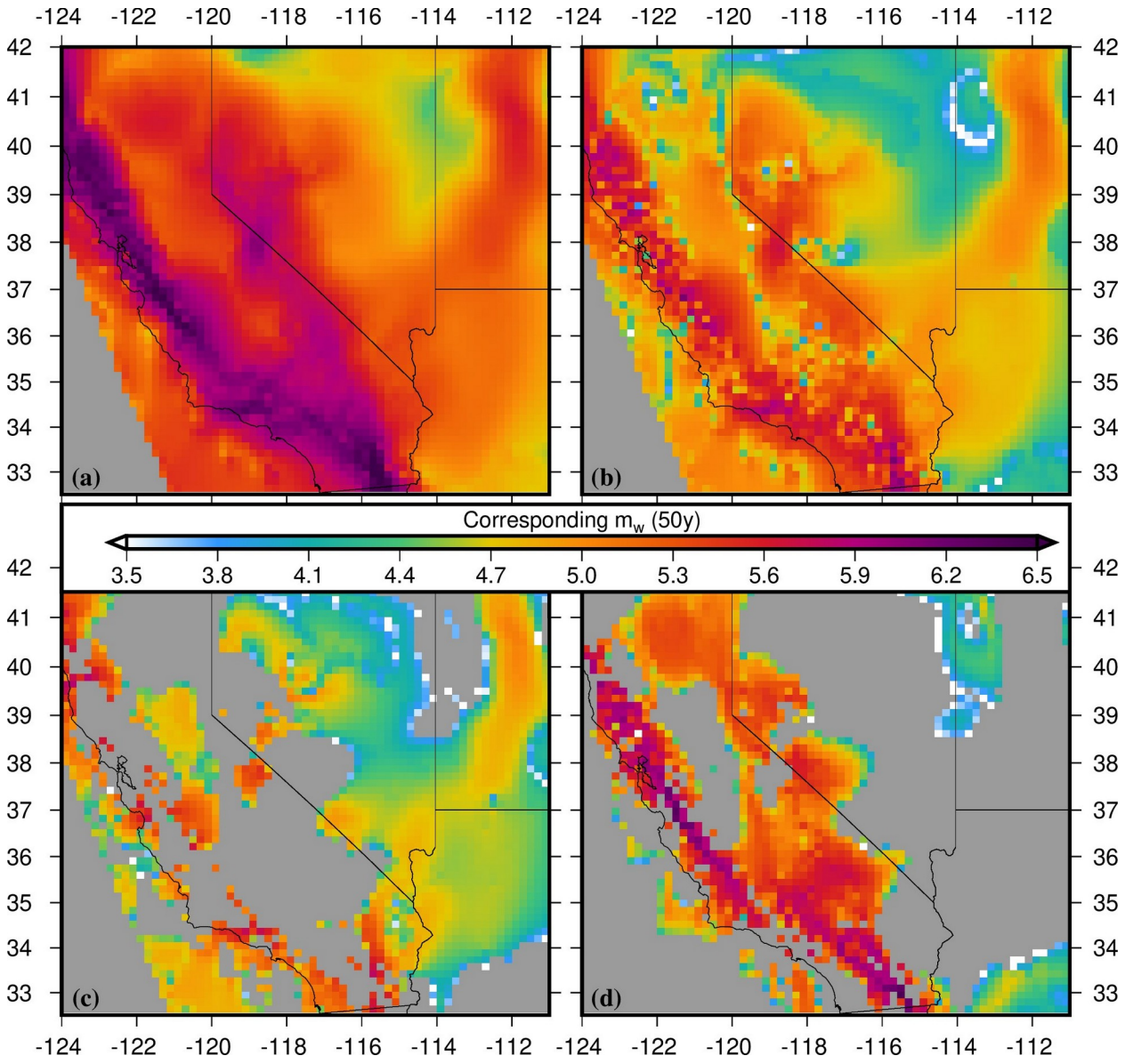


Figure 6. We define $M_{split} = \dot{M}_{split} T$, $M_{min} = \dot{M}_{min} T$, and $M_f = \dot{M}_f T$, and set T=50 years, D=15 km, and μ=30 GPa. For each grid cell (with given area) we then calculate (a) M_{split} and express it as the corresponding m_w, (b) m_w corresponding to the difference M_{split} - M_{min}, (c) m_w corresponding to the difference M_{split} - M_f, when $M_{split} > M_f$, (d) m_w corresponding to $|M_f - M_{split}|$, when $M_f > M_{split}$.

DATA AVAILABILITY STATEMENT

No new data were generated or analysed in support of this research. The strain rate model used in Section 7 is from Kreemer & Young (2022).

REFERENCES

Anderson, E. M. (1905). The dynamics of faulting. *Transactions of the Edinburgh Geological Society*, *8*(3), 387–402. https://doi.org/10.1144/transed.8.3.387

Anderson, E. M. (1951). *The dynamics of faulting and dyke formation with applications to Britain* (2nd ed., rev.). Edinburgh: Oliver and Boyd.

Bird, P., & Kreemer, C. (2015). Revised tectonic forecast of global shallow seismicity based on version 2.1 of the Global Strain Rate Map. *Bulletin of the Seismological Society of America*, *105*(1), 152–166. https://doi.org/10.1785/0120140129

Bird, P., & Liu, Z. (2007). Seismic hazard inferred from tectonics: California. *Seismological Research Letters*, *78*(1), 37–48. https://doi.org/10.1785/gssrl.78.1.37

Bird, P., Kreemer, C., & Holt, W. E. (2010). A long-term forecast of shallow seismicity based on the global strain rate map. *Seismological Research Letters*, *81*(2), 184–194. https://doi.org/10.1785/gssrl.81.2.184

Bird, P., Jackson, D. D., Kagan, Y. Y., Kreemer, C., & Stein, R. S. (2015). GEAR1: A Global Earthquake Activity Rate model constructed from geodetic strain rates and smoothed seismicity. *Bulletin of the Seismological Society of America*, *105*(5), 2538–2554. https://doi.org/10.1785/0120150058

Blewitt, G., Hammond, W. C., & Kreemer, C. (2005). Relating geothermal resources to Great Basin tectonics using GPS. *Geothermal Resources Council Transactions*, *29*, 331–335.

Blewitt, G., Hammond, W. C., & Kreemer, C. (2018). Harnessing the GPS data explosion for interdisciplinary science. *Eos*, *99*. https://doi.org/10.1029/2018EO104623

Bos, A. G., Spakman, W., & Nyst, M. C. J. (2003). Surface deformation and tectonic setting of Taiwan inferred from a GPS velocity field. *Journal of Geophysical Research: Solid Earth*, *108*(B10). https://doi.org/10.1029/2002JB002336

Calais, E., Dong, L., Wang, M., Shen, Z., & Vergnolle, M. (2006). Continental deformation in Asia from a combined GPS solution. *Geophysical Research Letters*, *33*(24), L24319. https://doi.org/10.1029/2006GL028433

Castro-Perdomo, N., Jónsson, S., Klinger, Y., Masson, F., Becker, T. W., & Johnson, K. (2025). Strain Rates Along the Alpine-Himalayan Belt From a Comprehensive GNSS Velocity Field. *Journal of Geophysical Research: Solid Earth*, *130*(12), e2025JB031738. https://doi.org/10.1029/2025JB031738

Cauchy, A. (1827). De la pression ou tension dans un corps solide. *Exercices de Mathématiques*, *2*, 42–56.

Célérier, B. (2008). Seeking Anderson's faulting in seismicity: A centennial celebration. *Reviews of Geophysics*, *46*(4). https://doi.org/10.1029/2007RG000240

Donniol Jouve, B., Socquet, A., Beauval, C., Piña Valdès, J., & Danciu, L. (2024). Consistency between the Strain Rate Model and ESHM20 Earthquake Rate Forecast in Europe: insights for seismic hazard. *EGUsphere*, 1–32. https://doi.org/10.5194/egusphere-2024-787

England, P., & Molnar, P. (2005). Late Quaternary to decadal velocity fields in Asia. *Journal of Geophysical Research: Solid Earth*, *110*(B12). https://doi.org/10.1029/2004JB003541

Faulds, J. E., Hinz, N., Kreemer, C., & Coolbaugh, M. (2012). Regional patterns of geothermal activity in the Great Basin region, western USA: Correlation with strain rates. *Transactions - Geothermal Resources Council*, *36*, 897–902.

Frank, F. C. (1966). Deduction of earth strains from survey data. *Bulletin of the Seismological Society of America*, *56*(1), 35–42.

Frohlich, C. (2001). Display and quantitative assessment of distributions of earthquake focal mechanisms. *Geophysical Journal International*, *144*(2), 300–308. https://doi.org/10.1046/j.1365-246x.2001.00341.x

Frohlich, C. (2007). Practical suggestions for assessing rates of seismic-moment release. *Bulletin of the Seismological Society of America*, *97*(4), 1158–1166. https://doi.org/10.1785/0120060193

Gordon, R. G., & Houseman, G. A. (2015). Deformation of Indian Ocean lithosphere: Evidence for a highly nonlinear rheological law. *Journal of Geophysical Research: Solid Earth*, *120*, 4434–4449. https://doi.org/10.1002/2015JB011993

Goudarzi, M. A., Cocard, M., & Santerre, R. (2015). GeoStrain: An open source software for calculating crustal strain rates. *Computers & Geosciences*, *82*, 1–12. https://doi.org/10.1016/j.cageo.2015.05.007

Haines, A. J., Dimitrova, L. L., Wallace, L. M., & Williams, C. A. (2015). *Enhanced Surface Imaging of Crustal Deformation: Obtaining Tectonic Force Fields Using GPS Data*. Springer.

Hanks, T. C., & Kanamori, H. (1979). A moment magnitude scale. *Journal of Geophysical Research: Solid Earth*, *84*(B5), 2348–2350. https://doi.org/10.1029/JB084iB05p02348

Hatem, A. E., Briggs, R. W., Pollitz, F. F., Reitman, N. G., & Tan, M. M. (2026). How to Determine an Earthquake Rate Budget? A Comparison of Geodetic, Geologic, and Seismologic Moment Rates. *Bulletin of the Seismological Society of America*. https://doi.org/10.1785/0120250228

Hill, R. (1952). On discontinuous plastic states, with special reference to localized necking in thin sheets. *Journal of the Mechanics and Physics of Solids*, *1*(1), 19–30. https://doi.org/10.1016/0022-5096(52)90003-3

Hirschberg, H., & Sutherland, R. (2024). Dynamical Modeling of Fault Slip Rates at the New Zealand Plate Boundary Indicates Fault Weakness. *Journal of Geophysical Research: Solid Earth*, *129*(4), e2023JB027806. https://doi.org/10.1029/2023JB027806

Holt, W. E., & Haines, A. J. (1993). Velocity fields in deforming Asia from the inversion of earthquake-released strains. *Tectonics*, *12*(1), 1–20. https://doi.org/10.1029/92TC00658

Holt, W. E., Chamot-Rooke, N., Le Pichon, X., Haines, A. J., Shen-Tu, B., & Ren, J. (2000). Velocity field in Asia inferred from Quaternary fault slip rates and Global Positioning System observations. *Journal of Geophysical Research*, *105*, 19,185-19,209.

Holt, W. E., Li, M., & Haines, A. J. (1995). Earthquake strain rates and instantaneous relative motions within central and eastern Asia. *Geophysical Journal International*, *122*(2), 569–593. https://doi.org/10.1111/j.1365-246X.1995.tb07014.x

Houseman, G., & England, P. (1986). Finite strain calculations of continental deformation: 1. Method and general results for convergent zones. *Journal of Geophysical Research*, *91*(B3), 3651–3663. https://doi.org/10.1029/JB091iB03p03651

Jackson, J., Haines, J., & Holt, W. (1994). A comparison of satellite laser ranging and seismicity data in the Aegean region. *Geophysical Research Letters*, *21*, 2849–2852.

Jaeger, J., Cook, N. G. W., & Zimmerman, R. (2007). *Fundamentals of Rock Mechanics* (4th edition). Malden, MA: Wiley-Blackwell.

Jenny, S., Goes, S., Giardini, D., & Kahle, H. G. (2004). Earthquake recurrence parameters from seismic and geodetic strain rates in the eastern Mediterranean. *Geophys. J. Int.*, *157*(3), 1331–1347.

Johnson, K. M. (2024). Disagreements in Geodetically Inferred Strain Rates in the Western US With Stress Orientations and Geologic Moment Rates. *Journal of Geophysical Research: Solid Earth*, *129*(4), e2023JB027472. https://doi.org/10.1029/2023JB027472

King, G., Klinger, Y., Bowman, D., & Tapponnier, P. (2005). Slip-Partitioned Surface Breaks for the Mw 7.8 2001 Kokoxili Earthquake, China. *Bulletin of the Seismological Society of America*, *95*(2), 731–738. https://doi.org/10.1785/0120040101

Klein, E. C., Flesch, L. M., Holt, W. E., & Haines, A. J. (2009). Evidence of long-term weakness on seismogenic faults in western North America from dynamic modeling. *Journal of Geophysical Research: Solid Earth*, *114*(B3). https://doi.org/10.1029/2007JB005201

Kostrov, V. V. (1974). Seismic moment and energy of earthquakes, and seismic flow of rocks. *Izv. Earth Physics*, *1*, 23–40.

Kreemer, C, & Young, Z. M. (2022). Crustal strain rates in the Western U.S. and their relationship with earthquake rates. *Seismological Research Letters*, *93*, 2990–3008.

Kreemer, C., Holt, W. E., Goes, S., & Govers, R. (2000). Active deformation in eastern Indonesia and the Philippines from GPS and seismicity data. *Journal of Geophysical Research - Solid Earth*, *105*(B1), 663–680.

Kreemer, C., Holt, W. E., & Haines, A. J. (2002). The global moment rate distribution within plate boundary zones. In S. Stein & J. T. Freymueller (Eds.), *Plate Boundary Zones* (pp. 173–190). Washington D.C.: American Geophysical Union.

Kreemer, C., Blewitt, G., & Hammond, W. C. (2006). Using geodesy to explore correlations between crustal deformation characteristics and geothermal resources. *Geothermal Resources Council Transactions*, *30*, 441–446.

Kreemer, C., Blewitt, G., & Klein, E. C. (2014). A geodetic plate motion and Global Strain Rate Model. *Geochemistry, Geophysics, Geosystems*, *15*(10), 3849–3889. https://doi.org/10.1002/2014GC005407

Kreemer, C., Hammond, W. C., & Blewitt, G. (2018). A Robust Estimation of the 3-D Intraplate Deformation of the North American Plate From GPS. *Journal of Geophysical Research: Solid Earth*, *123*(5), 4388–4412. https://doi.org/10.1029/2017JB015257

Kreemer, C., Blewitt, G., & Davis, P. M. (2020). Geodetic evidence for a buoyant mantle plume beneath the Eifel volcanic area, NW Europe. *Geophysical Journal International*, *222*(2), 1316–1332. https://doi.org/10.1093/gji/ggaa227

Kreemer, C., Zaliapin, I., & Kraaijpoel, D. (2024). On the Use of GNSS-Inferred Crustal Strain Accumulation in Evaluating Seismic Potential. In Y. Aoki & C. Kreemer (Eds.), *GNSS Monitoring of the Terrestrial Environment - Earthquakes, Volcanoes and Climate Change* (pp. 41–63). Elsevier.

Kreemer, C., Holt, W. E., & Haines, A. J. (2003). An integrated global model of present-day plate motions and plate boundary deformation. *Geophysical Journal International*, *154*(1), 8–34. https://doi.org/10.1046/j.1365-246X.2003.01917.x

Le, K., Lee, J., Owen, L. A., & Finkel, R. (2007). Late Quaternary slip rates along the Sierra Nevada frontal fault zone, California: Slip partitioning across the western margin of the Eastern California Shear Zone–Basin and Range Province. *GSA Bulletin*, *119*(1–2), 240–256. https://doi.org/10.1130/B25960.1

Lewis, J. C. (2007). Fine-scale partitioning of contemporary strain in the southern Walker Lane: Implications for accommodating divergent strike-slip motion. *Journal of Structural Geology*, *29*(7), 1201–1215. https://doi.org/10.1016/j.jsg.2007.02.015

Li, Y., Shan, X., Qu, C., Zhang, Y., Song, X., Jiang, Y., et al. (2017). Elastic block and strain modeling of GPS data around the Haiyuan-Liupanshan fault, northeastern Tibetan Plateau. *Journal of Asian Earth Sciences*, *150*, 87–97. https://doi.org/10.1016/j.jseaes.2017.10.010

Love, A. (1927). *A Treatise on the Mathematical Theory of Elasticity* (4th ed.). Cambridge University Press.

Luo, H., & Wang, T. (2022). Strain Partitioning on the Western Haiyuan Fault System Revealed by the Adjacent 2016 Mw5.9 and 2022 Mw6.7 Menyuan Earthquakes. *Geophysical Research Letters*, *49*(16), e2022GL099348. https://doi.org/10.1029/2022GL099348

Männel, B., Kreemer, C., & Cheng, G. (2026). Assessing small-scale surface deformation zones using GNSS-based imaging: a case-study for Europe. *Geophysical Journal International*, ggag461. https://doi.org/10.1093/gji/ggag461

Masson, F., Chéry, J., Hatzfeld, D., Martinod, J., Vernant, P., Tavakoli, F., & Ghafory-Ashtiani, M. (2005). Seismic versus aseismic deformation in Iran inferred from earthquakes and geodetic data. *Geophysical Journal International*, *160*(1), 217–226. https://doi.org/10.1111/j.1365-246X.2004.02465.x

Masson, Frédéric, Lehujeur, M., Ziegler, Y., & Doubre, C. (2014). Strain rate tensor in Iran from a new GPS velocity field. *Geophysical Journal International*, *197*(1), 10–21. https://doi.org/10.1093/gji/ggt509

Maurer, J., & Materna, K. (2023). Quantification of geodetic strain rate uncertainties and implications for seismic hazard estimates. *Geophysical Journal International*, *234*(3), 2128–2142. https://doi.org/10.1093/gji/ggad191

Maurer, J., Johnson, K., Wallace, L. M., Hamling, I., Williams, C. A., Rollins, C., et al. (2023). Geodetic Strain Rates for the 2022 Update of the New Zealand National Seismic Hazard Model. *Bulletin of the Seismological Society of America*, *114*(1), 57–77. https://doi.org/10.1785/0120230145

McCaffrey, R. (1997). Statistical significance of the seismic coupling coefficient. *Bulletin of the Seismological Society of America*, *87*(4), 1069–1073.

Métois, M., Lasserre, C., Méridi, A., Henriquet, M., & Bodin, T. (2025). Bayesian Estimation of Surface Strain Rates in the Peri-Adriatic, Balkans and Aegean region from GNSS Velocities. *Τεκτονικα*, *3*(1), 82–98. https://doi.org/10.55575/tektonika2025.3.1.99

Middleton, T., Parsons, B., & Walker, R. (2018). Comparison of seismic and geodetic strain rates at the margins of the Ordos Plateau, northern China. *Geophysical Journal International*, *212*(2), 988–1009.

Neha, Chuang, R. Y., Nishimura, T., Lee, Z., & Gao, J.-C. (2025). Balancing of geodetic and seismic moment rates and its implications for probabilistic seismic hazard analysis in Taiwan. *Earth, Planets and Space*, *77*(1), 125. https://doi.org/10.1186/s40623-025-02247-0

Nishimura, T. (2022). Time-independent forecast model for large crustal earthquakes in southwest Japan using GNSS data. *Earth, Planets and Space*, *74*(1), 58. https://doi.org/10.1186/s40623-022-01622-5

Nucci, R., Serpelloni, E., Faenza, L., Garcia, A., & Belardinelli, M. E. (2025). Geodetic Strain Rates and Seismicity Rates Along the Apennines (Italy). *Journal of Geophysical Research: Solid Earth*, *130*(2), e2024JB029848. https://doi.org/10.1029/2024JB029848

Okazaki, T., Fukahata, Y., & Nishimura, T. (2021). Consistent estimation of strain-rate fields from GNSS velocity data using basis function expansion with ABIC. *Earth, Planets and Space*, *73*(1), 153. https://doi.org/10.1186/s40623-021-01474-5

Pagani, C., Bodin, T., Métois, M., & Lasserre, C. (2021). Bayesian Estimation of Surface Strain Rates From Global Navigation Satellite System Measurements: Application to the Southwestern United States. *Journal of Geophysical Research: Solid Earth*, *126*(6), e2021JB021905. https://doi.org/10.1029/2021JB021905

Pancha, A., Anderson, J. G., & Kreemer, C. (2006). Comparison of seismic and geodetic scalar moment rates across the Basin and Range province. *Bulletin of the Seismological Society of America*, *96*, 11–32.

Pope, A. J. (1966). *Strain analysis of repeated triangulation for the investigation of crustal movement*. The Ohio State University.

Ranalli, G. (1995). *Rheology of the Earth* (2nd edition). London , UK: Springer.

Rashidi, A., & Derakhshani, R. (2022). Strain and Moment Rates from GPS and Seismological Data in Northern Iran: Implications for an Evaluation of Stress Trajectories and Probabilistic Fault Rupture Hazard. *Remote Sensing*, *14*(9). https://doi.org/10.3390/rs14092219

Rhoades, D. A., Christophersen, A., & Gerstenberger, M. C. (2017). Multiplicative earthquake likelihood models incorporating strain rates. *Geophysical Journal International*, *208*(3), 1764–1774. https://doi.org/10.1093/gji/ggw486

Rong, Y., Bird, P., & Jackson, D. D. (2016). Earthquake potential and magnitude limits inferred from a geodetic strain-rate model for southern Europe. *Geophysical Journal International*, *205*(1), 509–522. https://doi.org/10.1093/gji/ggw018

Roscoe, K. H. (1970). The Influence of Strains in Soil Mechanics. *Géotechnique*, *20*(2), 129–170. https://doi.org/10.1680/geot.1970.20.2.129

Sandwell, D. T., & Wessel, P. (2016). Interpolation of 2-D vector data using constraints from elasticity. *Geophysical Research Letters*, *43*(20), 10,703-10,709. https://doi.org/10.1002/2016GL070340

Savage, J. C., & Simpson, R. W. (1997). Surface strain accumulation and the seismic moment tensor. *Bulletin of the Seismological Society of America*, *87*(5), 1345–1353.

Shen, Z., Wang, M., Zeng, Y., & Wang, F. (2015). Optimal Interpolation of Spatially Discretized Geodetic Data. *Bulletin of the Seismological Society of America*, *105*(4), 2117–2127. https://doi.org/10.1785/0120140247

Shen-Tu, B., Holt, W. E., & Haines, A. J. (1995). Intraplate deformation in the Japanese Islands: A kinematic study of intraplate deformation at a convergent plate margin. *Journal of Geophysical Research: Solid Earth*, *100*(B12), 24275–24293. https://doi.org/10.1029/95JB02842

Shen-Tu, B., Holt, W. E., & Haines, A. J. (1998). Contemporary kinematics of the western United States determined from earthquake moment tensors, very long baseline interferometry, and GPS observations. *J. Geophys. Res.*, *103*(B8), 18,087-18,117.

Stevens, V. L., & Avouac, J.-P. (2021). On the relationship between strain rate and seismicity in the India–Asia collision zone: implications for probabilistic seismic hazard. *Geophysical Journal International*, *226*(1), 220–245. https://doi.org/10.1093/gji/ggab098

Stören, S., & Rice, J. R. (1975). Localized necking in thin sheets. *Journal of the Mechanics and Physics of Solids*, *23*(6), 421–441. https://doi.org/10.1016/0022-5096(75)90004-6

Tape, C., Musé, P., Simons, M., Dong, D., & Webb, F. (2009). Multiscale estimation of GPS velocity fields. *Geophysical Journal International*, *179*(2), 945–971. https://doi.org/10.1111/j.1365-246X.2009.04337.x

Taroni, M., & Carafa, M. M. C. (2023). Earthquake size distributions are slightly different in compression vs extension. *Communications Earth & Environment*, *4*(1), 1–10. https://doi.org/10.1038/s43247-023-01059-y

Ward, S. N. (1994). A multidisciplinary approach to seismic hazard in southern California. *Bulletin of the Seismological Society of America*, *84*(5), 1293–1309.

Ward, S. N. (1998). On the consistency of earthquake moment rates, geological fault data, and space geodetic strain: the United States. *Geophys. J. Int.*, *134*(1), 172–186.

Wei, C., Meng, G., Wu, W., Chen, X., Zhang, M., Zhao, G., et al. (2023). Time-Independent Grid-Based Forecast Model for M ≥6.0 Earthquakes in Southeastern Tibetan Plateau Using GNSS Strain Rates and Seismicity. *Bulletin of the Seismological Society of America*, *114*(1), 258–277. https://doi.org/10.1785/0120230152

Wessel, P., Luis, J. F., Uieda, L., Scharroo, R., Wobbe, F., Smith, W. H. F., & Tian, D. (2019). The Generic Mapping Tools Version 6. *Geochemistry, Geophysics, Geosystems*, *20*(11), 5556–5564. https://doi.org/10.1029/2019GC008515

Working Group on California Earthquake Probabilities. (1995). Seismic hazards in Southern California: Probable earthquakes, 1994 to 2024. *Bulletin of the Seismological Society of America*, *85*(2), 379–439. https://doi.org/10.1785/BSSA0850020379

Wu, Y., Jiang, Z., Yang, G., Wei, W., & Liu, X. (2011). Comparison of GPS strain rate computing methods and their reliability. *Geophysical Journal International*, *185*(2), 703–717. https://doi.org/10.1111/j.1365-246X.2011.04976.x

Yuliastuti, Y., Meilano, I., Puspito, N. T., Susilo, S., & Setyadji, A. B. (2026). Seismicity-rate estimation based on geodetic strain rates from continuous GNSS observations in Kalimantan, Indonesia. *Earth, Planets and Space*, *78*(1), 89. https://doi.org/10.1186/s40623-026-02392-0

Zaliapin, I., & Ben-Zion, Y. (2016). A global classification and characterization of earthquake clusters. *Geophysical Journal International*, *207*(1), 608–634. https://doi.org/10.1093/gji/ggw300

Zaliapin, I. V., Kagan, Y. Y., & Schoenberg, F. P. (2005). Approximating the distribution of Pareto sums. *Pure and Applied Geophysics*, *162*(6–7), 1187–1228. https://doi.org/10.1007/s00024-004-2666-3

Zeng, Y., Petersen, M. D., & Shen, Z.-K. (2018). Earthquake potential in California-Nevada implied by correlation of strain rate and seismicity. *Geophysical Research Letters*, *45*(4), 1778–1785. https://doi.org/10.1002/2017GL075967

Zheng, G., Lou, Y., Wang, H., Geng, J., & Shi, C. (2018). Shallow Seismicity Forecast for the India-Eurasia Collision Zone Based on Geodetic Strain Rates. *Geophysical Research Letters*, *45*(17), 8905–8912. https://doi.org/10.1029/2018GL078814

APPENDIX A: Derivation of $\dot{\varepsilon}_s$ from Zero-Length-Change Orientations

A.1. Zero-length-change orientations

Tensor form. For a unit vector $\boldsymbol{t}=(\cos\theta,\sin\theta)$, with θ measured counter-clockwise from east, the strain rate in the direction of $\boldsymbol{t}$, i.e., the fractional rate of length change of a line element along $\boldsymbol{t}$, is (Jaeger et al., 2007):

$$\dot{\varepsilon}_{tt}=\boldsymbol{t}^{T}\,\dot{\boldsymbol{\varepsilon}}\,\boldsymbol{t}=\dot{\varepsilon}_{xx}\cos^2\theta+2\,\dot{\varepsilon}_{xy}\sin\theta\cos\theta+\dot{\varepsilon}_{yy}\sin^2\theta \tag{A1}$$

A zero-length-change (ZLC) orientation $\boldsymbol{t}_{\mathrm{ZLC}}$ is a direction in which there is no length change, $\dot{\varepsilon}_{tt}=0$. We therefore set (A1) to zero and divide it by $\cos^2\theta$:

$$\dot{\varepsilon}_{yy}\tan^2\theta+2\,\dot{\varepsilon}_{xy}\tan\theta+\dot{\varepsilon}_{xx}=0 \tag{A2}$$

with solutions ($\theta=\theta_{ZLC}$):

$$\tan\theta_{ZLC}=\frac{-\dot{\varepsilon}_{xy}\pm\sqrt{\dot{\varepsilon}_{xy}^2-\dot{\varepsilon}_{xx}\dot{\varepsilon}_{yy}}}{\dot{\varepsilon}_{yy}} \tag{A3}$$

Real solutions exist when $\dot{\varepsilon}_{xy}^2\geq\dot{\varepsilon}_{xx}\dot{\varepsilon}_{yy}$. If $\dot{\varepsilon}_{yy}=0$, dividing by $\cos^2\theta$ loses the north-south orientation ($\theta=90°$), which is then itself a ZLC orientation; the other solution is $\tan\theta=-\dot{\varepsilon}_{xx}/(2\,\dot{\varepsilon}_{xy})$. Eq. (A3) is the same form as that derived by Holt & Haines (1993) (from different but related reasoning), who named these orientations “no-length-change”

Principal-axes form. In the principal frame ($\dot{\boldsymbol{\varepsilon}}=\mathrm{diag}(\dot{\varepsilon}_1,\dot{\varepsilon}_2)$), and for an angle ϕ measured counter-clockwise from the $\dot{\varepsilon}_1$ axis, (A1) reduces to:

$$\dot{\varepsilon}_1\cos^2\phi+\dot{\varepsilon}_2\sin^2\phi=0\Rightarrow\tan^2\phi=\frac{-\dot{\varepsilon}_1}{\dot{\varepsilon}_2} \tag{A4}$$

Real solutions exist only when $\dot{\varepsilon}_1\dot{\varepsilon}_2\leq 0$, i.e., when the principal strains have opposite signs (or one of them is zero). When both eigenvalues share a sign (the same-sign regime), no ZLC orientation exists — every material line is either lengthening or shortening. The two ZLC orientations are: $\phi_{ZLC}=\pm\arctan\sqrt{-\dot{\varepsilon}_1/\dot{\varepsilon}_2}$, which are symmetric about the principal axes. In terms of the geographic angle, the two solutions are $\theta_{\mathrm{ZLC}}=\alpha\pm\phi_{\mathrm{ZLC}}$, where α is the angle of the $\dot{\varepsilon}_1$ axis from the x axis (see (3), Figure 2). These are the same two orientations as the solutions of Eq. (A3), with $\alpha-\phi_{\mathrm{ZLC}}$ the plus root and $\alpha+\phi_{\mathrm{ZLC}}$ the minus root (the slip sense is given in A.2).

A.2. Dilatation and shear at a ZLC orientation

The strain rate components at a ZLC orientation are most easily found by rotating the principal axes counterclockwise by ϕ to a frame $(\boldsymbol{t},\boldsymbol{n})$. In that frame, $\boldsymbol{n}$ is rotated 90° counterclockwise from $\boldsymbol{t}$.

$$\dot{\boldsymbol{\varepsilon}}' = \boldsymbol{R}\begin{pmatrix}\dot{\varepsilon}_1 & 0\\ 0 & \dot{\varepsilon}_2\end{pmatrix}\boldsymbol{R}^T, \qquad \boldsymbol{R}(\phi)=\begin{pmatrix}\cos\phi & \sin\phi\\ -\sin\phi & \cos\phi\end{pmatrix}$$

With $\dot{\gamma}=\dot{\varepsilon}_1-\dot{\varepsilon}_2$, this gives:

$$\begin{pmatrix}\dot{\varepsilon}_{tt} & \dot{\varepsilon}_{tn}\\ \dot{\varepsilon}_{tn} & \dot{\varepsilon}_{nn}\end{pmatrix}=\begin{pmatrix}\dot{\varepsilon}_1\cos^2\phi+\dot{\varepsilon}_2\sin^2\phi & -\dot{\gamma}\sin\phi\cos\phi\\ -\dot{\gamma}\sin\phi\cos\phi & \dot{\varepsilon}_1\sin^2\phi+\dot{\varepsilon}_2\cos^2\phi\end{pmatrix} \tag{A5}$$

Note that $\dot{\varepsilon}_{tt}$ is expressed similarly to Eq. (A1), but now in principal terms.

At $\phi=\pm\phi_{\mathrm{ZLC}}$, $\boldsymbol{t}$ and $\boldsymbol{n}$ are the ZLC orientation $\boldsymbol{t}_{\mathrm{ZLC}}$ and its perpendicular $\boldsymbol{n}_{\mathrm{ZLC}}$. When we combine the ZLC condition $\dot{\varepsilon}_1\cos^2\phi_{\mathrm{ZLC}}+\dot{\varepsilon}_2\sin^2\phi_{\mathrm{ZLC}}=0$ (A4) with the trigonometric identity $\cos^2\phi_{\mathrm{ZLC}}+\sin^2\phi_{\mathrm{ZLC}}=1$ we obtain solutions $\cos^2\phi_{\mathrm{ZLC}}=-\dot{\varepsilon}_2/\dot{\gamma}$ and $\sin^2\phi_{\mathrm{ZLC}}=\dot{\varepsilon}_1/\dot{\gamma}$ (for $\dot{\varepsilon}_1\dot{\varepsilon}_2\le 0$). Substituting those into (A5) gives:

$$\dot{\varepsilon}_{tt}=0, \qquad \dot{\varepsilon}_{nn}=\frac{\dot{\varepsilon}_1^2-\dot{\varepsilon}_2^2}{\dot{\gamma}}=\dot{\varepsilon}_1+\dot{\varepsilon}_2=\dot{\varepsilon}_d \tag{A6}$$

So, $\dot{\varepsilon}_{tt}=0$ recovers the definition of a ZLC orientation, and the full dilatation rate acts in the direction $\boldsymbol{n}_{\mathrm{ZLC}}$ with none along $\boldsymbol{t}_{\mathrm{ZLC}}$: a clean kinematic partition of the tensor in the fault frame: no normal strain in the shear term, and no shear in the normal-strain term. The shear component is:

$$\dot{\varepsilon}_{tn}^2=\dot{\gamma}^2\sin^2\phi_{\mathrm{ZLC}}\cos^2\phi_{\mathrm{ZLC}}=-\dot{\varepsilon}_1\dot{\varepsilon}_2 \tag{A7}$$

which is consistent with the invariance of the determinant, $-\dot{\varepsilon}_{\mathrm{tn}}^2=\det(\dot{\boldsymbol{\varepsilon}})=\dot{\varepsilon}_1\dot{\varepsilon}_2$. Therefore,

$$|\dot{\varepsilon}_{tn}|=\sqrt{-\dot{\varepsilon}_1\dot{\varepsilon}_2} \tag{A8}$$

which is real only when $\dot{\varepsilon}_1\dot{\varepsilon}_2\le 0$, the condition for a ZLC orientation to exist (A.1). This is the tensorial shear strain rate on the ZLC orientation, determined uniquely by the two principal strain rates through their product. The corresponding engineering shear strain rate, twice the tensorial component, is

$$\dot{\varepsilon}_s=2|\dot{\varepsilon}_{tn}|=2\sqrt{-\dot{\varepsilon}_1\dot{\varepsilon}_2} \quad (\dot{\varepsilon}_1\dot{\varepsilon}_2\le 0), \qquad \dot{\varepsilon}_s=0 \quad (\dot{\varepsilon}_1\dot{\varepsilon}_2>0) \tag{A9}$$

As a check, for simple shear $u=\dot{\gamma}\ y$, $v=0$ (the same strain rate tensor results from pure shear), $\dot{\varepsilon}_{xy}=\dot{\gamma}/2$ and $\dot{\varepsilon}_1=-\dot{\varepsilon}_2=\dot{\gamma}/2$, so Eq. (A9) gives $\dot{\varepsilon}_s=\dot{\gamma}$: $\dot{\varepsilon}_s$ reproduces the engineering shear strain rate, which confirms the factor of two between $\dot{\varepsilon}_{tn}$ and $\dot{\varepsilon}_s$.

From (A5), $\dot{\varepsilon}_{tn}=-\dot{\gamma}\sin\phi\cos\phi$, so $\dot{\varepsilon}_{tn}=\mp\sqrt{-\dot{\varepsilon}_1\dot{\varepsilon}_2}$ at $\phi=\pm\phi_{\mathrm{ZLC}}$. The sign of $\dot{\varepsilon}_{tn}$ is the slip sense: positive for right-lateral and negative for left-lateral slip. The right-lateral orientation is

therefore $\alpha-\phi_{\mathrm{ZLC}}$ and the left-lateral one $\alpha+\phi_{\mathrm{ZLC}}$. In geographic components, $\dot{\varepsilon}_{tn}=(\dot{\varepsilon}_{yy}-\dot{\varepsilon}_{xx})\sin\theta\cos\theta+\dot{\varepsilon}_{xy}(\cos^2\theta-\sin^2\theta)$, which reduces with Eq. (A2) to $\dot{\varepsilon}_{tn}=\dot{\varepsilon}_{xy}+\dot{\varepsilon}_{yy}\tan\theta=\pm\sqrt{\dot{\varepsilon}_{xy}^2-\dot{\varepsilon}_{xx}\dot{\varepsilon}_{yy}}=\pm\dot{\varepsilon}_s/2$ at the roots of Eq. (A3). The plus root of Eq. (A3) is therefore the right-lateral orientation and the minus root the left-lateral one. If $\dot{\varepsilon}_{yy}=0$, the north-south orientation has $\dot{\varepsilon}_{tn}=-\dot{\varepsilon}_{xy}$ and the other root has $+\dot{\varepsilon}_{xy}$, so which of them is right-lateral then depends on the sign of $\dot{\varepsilon}_{xy}$.

In the frame $(\boldsymbol{t}_{\mathrm{ZLC}},\boldsymbol{n}_{\mathrm{ZLC}})$ the tensor separates into a strike-slip part and a dilatational part:

$$\begin{pmatrix} 0 & \dot{\varepsilon}_{\mathrm{tn}} \\ \dot{\varepsilon}_{\mathrm{tn}} & \dot{\varepsilon}_d \end{pmatrix}=\begin{pmatrix} 0 & \dot{\varepsilon}_{\mathrm{tn}} \\ \dot{\varepsilon}_{\mathrm{tn}} & 0 \end{pmatrix}+\begin{pmatrix} 0 & 0 \\ 0 & \dot{\varepsilon}_d \end{pmatrix}$$

The first term is the contribution of a strike-slip fault along the ZLC orientation: shear only, with no strain rate along or across the fault. The second term is the dilatation, which acts across the fault in the direction $\boldsymbol{n}_{\mathrm{ZLC}}$. It cannot be accommodated by strike-slip motion and is attributed to dip-slip faults (Appendix D).

A.3. Invariance and uniqueness

Within the construction of A.2, a shear tensor along a fault plus a single normal strain across it, the amplitudes $\dot{\varepsilon}_s$ in Eq. (A9) and $\dot{\varepsilon}_d$ do not depend on any choice made in deriving them. This is uniqueness within the construction; it does not establish a unique fault population (Section 6).

Choice of ZLC orientation. There are two ZLC orientations, $\phi=\pm\phi_{\mathrm{ZLC}}$. Both give the same $|\dot{\varepsilon}_{\mathrm{tn}}|$ (A7), and therefore the same $\dot{\varepsilon}_s$ and $\dot{\varepsilon}_d$, although the tensors assigned to the two modes differ.

Choice of coordinate system. $\dot{\varepsilon}_s$ depends only on the product $\dot{\varepsilon}_1\dot{\varepsilon}_2$, which equals the determinant of the tensor (i.e., $\dot{\varepsilon}_s=2\sqrt{-\det(\dot{\boldsymbol{\varepsilon}})}$ when $\dot{\varepsilon}_1\dot{\varepsilon}_2\le 0$). It is therefore the same in every frame.

Choice of fault orientation. At an arbitrary orientation ϕ, (A5) gives the strain rate along it as $\dot{\varepsilon}_{tt}=\dot{\varepsilon}_d/2+(\dot{\gamma}/2)\cos 2\phi$ and across it as $\dot{\varepsilon}_{\mathrm{nn}}=\dot{\varepsilon}_d/2-(\dot{\gamma}/2)\cos 2\phi$. Removing the shear $\dot{\varepsilon}_{tn}$ therefore leaves a remainder with non-zero strain rates both along and across the fault. Only at the ZLC orientations, where $\cos 2\phi_{\mathrm{ZLC}}=-\dot{\varepsilon}_d/\dot{\gamma}$ is $\dot{\varepsilon}_{tt}=0$. The remainder is then the single dilatation $\dot{\varepsilon}_d$ acting across the fault (A6), which can be assigned to one set of dip-slip faults, as the partition requires.

Same-sign regime. When the principal strain rates share a sign there is no ZLC orientation, and $\dot{\varepsilon}_s=0$ is the extension of the definition (A9). It is a convention, not an observation that strike-slip faulting is absent.

A.4. Mohr circle coordinates and the ZLC angle

For a plane whose normal $\boldsymbol{n}$ makes angle ϕ with the $\dot{\varepsilon}_1$ axis, the trace $\boldsymbol{t}$ is at $\phi-90°$, since $\boldsymbol{n}$ rotated 90° counterclockwise from $\boldsymbol{t}$. Applying (A5) with $\phi-90°$ in place of ϕ, and using $\sin(\phi-90°)=-\cos\phi$ and $\cos(\phi-90°)=\sin\phi$, gives the coordinates of the plane on the Mohr circle in Section 4.1,

$$\dot{\varepsilon}_{nn}=\dot{\varepsilon}_1\cos^2\phi+\dot{\varepsilon}_2\sin^2\phi=\frac{\dot{\varepsilon}_d}{2}+\frac{\dot{\gamma}}{2}\cos 2\phi\,,\qquad \dot{\varepsilon}_{tn}=\frac{\dot{\gamma}}{2}\sin 2\phi \tag{A10}$$

The planes with no strain rate in the direction of their normal ($\dot{\varepsilon}_{nn}=0$) therefore have

$$\cos 2\phi_{\mathrm{ZLC}}=\frac{-\dot{\varepsilon}_d}{\dot{\gamma}} \tag{A11}$$

Using $\sin^2\phi=(1-\cos 2\phi)/2$ and $\cos^2\phi=(1+\cos 2\phi)/2$, $\tan^2\phi=(1-\cos 2\phi)/(1+\cos 2\phi)$, and with $\dot{\gamma}+\dot{\varepsilon}_d=2\dot{\varepsilon}_1$ and $\dot{\gamma}-\dot{\varepsilon}_d=-2\dot{\varepsilon}_2$,

$$\tan^2\phi_{\mathrm{ZLC}}=\frac{\dot{\gamma}+\dot{\varepsilon}_d}{\dot{\gamma}-\dot{\varepsilon}_d}=\frac{-\dot{\varepsilon}_1}{\dot{\varepsilon}_2} \tag{A12}$$

which is (A4): the Mohr circle and the rotation given in A.2 give the same ZLC orientations. For $\dot{\varepsilon}_1:\dot{\varepsilon}_2=3:-1$ (Figure 2), $\cos 2\phi_{\mathrm{ZLC}}=-1/2$, $\phi_{\mathrm{ZLC}}=60°$ and $\tan^2\phi_{\mathrm{ZLC}}=3=-\dot{\varepsilon}_1/\dot{\varepsilon}_2$.

Appendix B: Proof of Additivity of $\dot{\varepsilon}_t$

We show that $\dot{\varepsilon}_t=\dot{\varepsilon}_s+|\dot{\varepsilon}_d|$ satisfies the additivity property: the total strain rate of a deformation equals the sum of the total strain rates of its strike-slip and dilatational parts; we illustrate this with two modes applied independently and then combined.

Case *A* (pure uniaxial extension): $\dot{\varepsilon}_1=a$, $\dot{\varepsilon}_2=0$. Since $\dot{\varepsilon}_1\dot{\varepsilon}_2=0$, we have $\dot{\varepsilon}_s=0$, $\dot{\varepsilon}_d=a$, and $\dot{\varepsilon}_t^{(A)}=a$.

Case *B* (zero dilatation): $\dot{\varepsilon}_1=a/2$, $\dot{\varepsilon}_2=-a/2$. We have $\dot{\varepsilon}_d=0$, $\dot{\varepsilon}_s=2\sqrt{a^2/4}=a$, and $\dot{\varepsilon}_t^{(B)}=a$.

Case *C* (simultaneous combination): The combined strain tensor is:

$$\dot{\boldsymbol{\varepsilon}}=a\begin{pmatrix}0 & \frac{1}{2}\\ \frac{1}{2} & 1\end{pmatrix} \tag{B1}$$

with eigenvalues $\dot{\varepsilon}_1=a(1+\sqrt{2})/2$ and $\dot{\varepsilon}_2=a(1-\sqrt{2})/2$. Then:

$$\dot{\varepsilon}_d = a, \qquad \dot{\varepsilon}_s = 2\sqrt{-\dot{\varepsilon}_1\dot{\varepsilon}_2} = 2\sqrt{\frac{a^2(\sqrt{2}+1)(\sqrt{2}-1)}{4}} = 2\sqrt{\frac{a^2}{4}} = a \tag{B2}$$

Therefore $\dot{\varepsilon}_t^{(C)} = a + a = 2a = \dot{\varepsilon}_t^{(A)} + \dot{\varepsilon}_t^{(B)}$.

Scope of the additivity. For any strain rate tensor with a ZLC orientation (and using case C as an example), the partition in A.2 splits it into a dilatational part (case A), which acts across the fault, with $\dot{\varepsilon}_s^{(A)} = 0$ and $\dot{\varepsilon}_d^{(A)} = \dot{\varepsilon}_d$, and a strike-slip part (case B), with $\dot{\varepsilon}_d^{(B)} = 0$ and $\dot{\varepsilon}_s^{(B)} = \dot{\varepsilon}_s$. Hence $\dot{\varepsilon}_t^{(C)} = \dot{\varepsilon}_t^{(A)} + \dot{\varepsilon}_t^{(B)}$ for every such tensor, which is the definition $\dot{\varepsilon}_t = |\dot{\varepsilon}_d| + \dot{\varepsilon}_s$; the example above is one instance. The property is tied to this fault-frame partition and does not extend to arbitrary sums of tensors, because $\dot{\varepsilon}_s$ is not linear in the tensor: two shears with different ZLC orientations, or a dilatation along an axis that is not across a ZLC orientation of the shear, do not add, and canceling contributions reduce $\dot{\varepsilon}_t$. In particular $\dot{\varepsilon}_t$ is not a norm: it can violate the triangle inequality.

Appendix C: Uncertainties for Scalar Strain Rates and Moment Rate

We derive first-order standard deviations of the new definitions. The input quantities are the strain rate tensor components $\dot{\varepsilon}_{xx}$, $\dot{\varepsilon}_{yy}$, $\dot{\varepsilon}_{xy}$ with standard deviations σ_{xx}, σ_{yy}, σ_{xy}, which we assume to be uncorrelated. In general $\sigma_{xx} \neq \sigma_{yy}$ and the three uncertainties are independent quantities. The general propagation of errors for a function $g(\dot{\varepsilon}_{xx}, \dot{\varepsilon}_{yy}, \dot{\varepsilon}_{xy})$ of the tensor components (here $\dot{\varepsilon}_d$, $\dot{\varepsilon}_s$, $\dot{\varepsilon}_t$, Φ or $\dot{M}_{\text{split}}$) gives:

$$\sigma_g^2 = \left(\frac{\partial g}{\partial \dot{\varepsilon}_{xx}}\right)^2 \sigma_{xx}^2 + \left(\frac{\partial g}{\partial \dot{\varepsilon}_{yy}}\right)^2 \sigma_{yy}^2 + \left(\frac{\partial g}{\partial \dot{\varepsilon}_{xy}}\right)^2 \sigma_{xy}^2 \tag{C1}$$

If the covariance matrix of the components is available, the first-order variance of g is

$$\sigma_g^2 = \sum_i \sum_j \left(\frac{\partial g}{\partial \varepsilon_i}\right)\left(\frac{\partial g}{\partial \varepsilon_j}\right) \mathrm{cov}(\varepsilon_i, \varepsilon_j), \qquad i, j = xx, yy, xy$$

of which (C1) is the special case with only the diagonal terms. A positive correlation between $\dot{\varepsilon}_{xx}$ and $\dot{\varepsilon}_{yy}$, for example, increases σ_d, and a negative correlation decreases it.

Results are presented first in terms of tensor components (C.1), then in the more compact eigenvalue form (C.2).

C.1. Expressions in Terms of Tensor Components

Dilatation rate $\dot{\varepsilon}_d = \dot{\varepsilon}_{xx} + \dot{\varepsilon}_{yy}$:

$$\sigma_{\dot{\varepsilon}_d} = \sqrt{\sigma_{xx}^2 + \sigma_{yy}^2} \tag{C2}$$

Strike-slip strain rate $\dot{\varepsilon}_s = 2\sqrt{\dot{\varepsilon}_{xy}^2 - \dot{\varepsilon}_{xx}\,\dot{\varepsilon}_{yy}}$:

$$\sigma_{\dot{\varepsilon}_s} = \frac{2}{\dot{\varepsilon}_s}\sqrt{\dot{\varepsilon}_{yy}^2\ \sigma_{xx}^2 + \dot{\varepsilon}_{xx}^2\ \sigma_{yy}^2 + 4\,\dot{\varepsilon}_{xy}^2\ \sigma_{xy}^2} \tag{C3}$$

The factor $1/\dot{\varepsilon}_s$, which also appears in (C4) to (C6), causes the uncertainties to diverge as $\dot{\varepsilon}_s \to 0$, i.e., approaching the boundary between the opposite- and same-sign regimes ($|\Phi| = 1$), where ZLC orientations disappear. Because the first-order expressions become singular near the regime boundary, they should not be read as standard deviations where the uncertainty spans that boundary.

Total strain rate $\dot{\varepsilon}_t = \dot{\varepsilon}_s + |\dot{\varepsilon}_d| = \dot{\varepsilon}_s + s_d\,\dot{\varepsilon}_d$, where $s_d = sgn(\dot{\varepsilon}_d)$:

$$\sigma_{\dot{\varepsilon}_t}^2 = \left(s_d - \frac{2\,\dot{\varepsilon}_{yy}}{\dot{\varepsilon}_s}\right)^2 \sigma_{xx}^2 + \left(s_d - \frac{2\,\dot{\varepsilon}_{xx}}{\dot{\varepsilon}_s}\right)^2 \sigma_{yy}^2 + \left(\frac{4\,\dot{\varepsilon}_{xy}}{\dot{\varepsilon}_s}\right)^2 \sigma_{xy}^2 \tag{C4}$$

Style parameter $\Phi = \dot{\varepsilon}_d/\dot{\varepsilon}_t$, defined for $\dot{\varepsilon}_s > 0$ (the opposite-sign regime), where Φ has the sign of $\dot{\varepsilon}_d$ (the same-sign regime is treated in C.2):

$$\sigma_\Phi^2 = \frac{1}{\dot{\varepsilon}_t^2}\left[\left(1 - |\Phi| + \frac{2\,\Phi\,\dot{\varepsilon}_{yy}}{\dot{\varepsilon}_s}\right)^2 \sigma_{xx}^2 + \left(1 - |\Phi| + \frac{2\,\Phi\,\dot{\varepsilon}_{xx}}{\dot{\varepsilon}_s}\right)^2 \sigma_{yy}^2 + \left(\frac{4\,\Phi\,\dot{\varepsilon}_{xy}}{\dot{\varepsilon}_s}\right)^2 \sigma_{xy}^2\right] \tag{C5}$$

Moment rate $\dot{M}_{\text{split}} = \mu\,D\,A\,(\dot{\varepsilon}_s + f\,|\dot{\varepsilon}_d|)$, where f is the dip factor (Section 6.1):

$$\sigma_{\dot{M}_{\text{split}}}^2 = (\mu\,D\,A)^2\left[\left(f\,s_d - \frac{2\,\dot{\varepsilon}_{yy}}{\dot{\varepsilon}_s}\right)^2 \sigma_{xx}^2 + \left(f\,s_d - \frac{2\,\dot{\varepsilon}_{xx}}{\dot{\varepsilon}_s}\right)^2 \sigma_{yy}^2 + \left(\frac{4\,\dot{\varepsilon}_{xy}}{\dot{\varepsilon}_s}\right)^2 \sigma_{xy}^2\right] \tag{C6}$$

For $f = 1$, $\dot{M}_{\text{split}}/(\mu\,D\,A) = \dot{\varepsilon}_t$ and (C6) reduces to $(\mu\,D\,A)^2$ times (C4). The uncertainties of μ, D, A and δ, which also enter $\dot{M}_{\text{split}}$, are not included.

C.2. Expressions in Terms of Eigenvalue Uncertainties

Below are the same uncertainties, but now expressed in terms of the uncertainties of the principal strain rates ($\sigma_1 \equiv \sigma_{\dot{\varepsilon}_1}, \sigma_2 \equiv \sigma_{\dot{\varepsilon}_2}$). With $\dot{\gamma} = \dot{\varepsilon}_1 - \dot{\varepsilon}_2$, the uncertainty of $\dot{\varepsilon}_1$ is:

$$\sigma_1^2 = \frac{1}{4\,\dot{\gamma}^2}\left[(\dot{\varepsilon}_{xx} - \dot{\varepsilon}_{yy} + \dot{\gamma})^2 \sigma_{xx}^2 + (\dot{\varepsilon}_{xx} - \dot{\varepsilon}_{yy} - \dot{\gamma})^2 \sigma_{yy}^2 + 16\,\dot{\varepsilon}_{xy}^2 \sigma_{xy}^2\right] \tag{C7}$$

and that of $\dot{\varepsilon}_2$ follows from (C7) by replacing $\dot{\gamma}$ with $-\dot{\gamma}$. The two are equal if $\sigma_{xx}=\sigma_{yy}$. The covariance is:

$$C_{12}=\frac{\dot{\varepsilon}_{xy}^2}{\dot{\gamma}^2}\left(\sigma_{xx}^2+\sigma_{yy}^2-4\,\sigma_{xy}^2\right) \tag{C8}$$

With C_{12} and $r=-\dot{\varepsilon}_1/\dot{\varepsilon}_2$, the standard deviations of the various scalars are a function of σ_1^2 and σ_2^2 through the form: $\mathrm{var}\left(a\,\dot{\varepsilon}_1+b\,\dot{\varepsilon}_2\right)=a^2\sigma_1^2+b^2\sigma_2^2+2\,a\,b\;C_{12}$:

Quantity	a	b
$\dot{\varepsilon}_d$	1	1
$\dot{\varepsilon}_s$	$1/\sqrt{r}$	$-\sqrt{r}$
$\dot{\varepsilon}_t$	$s_d+1/\sqrt{r}$	$s_d-\sqrt{r}$
Φ ($\dot{\varepsilon}_s>0$)	$\left[1-\Phi\left(s_d+1/\sqrt{r}\right)\right]/\dot{\varepsilon}_t$	$\left[1-\Phi\left(s_d-\sqrt{r}\right)\right]/\dot{\varepsilon}_t$
Φ ($\dot{\varepsilon}_s=0$, extension)	$-\dot{\varepsilon}_2/\dot{\varepsilon}_1^2$	$1/\dot{\varepsilon}_1$
Φ ($\dot{\varepsilon}_s=0$, contraction)	$-1/\dot{\varepsilon}_2$	$\dot{\varepsilon}_1/\dot{\varepsilon}_2^2$
$\dot{M}_{\mathrm{split}}/(\mu\,D\,A)$	$f\,s_d+1/\sqrt{r}$	$f\,s_d-\sqrt{r}$

Appendix D: From Strain Rate to Scalar Seismic Moment — Kostrov, the Factor of Two, and the Definition of $\dot{M}_{\mathrm{split}}$

D.1. The Kostrov tensor relation and its factor of two

For a single fault with unit normal $\boldsymbol{n}$, unit slip direction $\boldsymbol{s}$ in the fault plane ($\boldsymbol{n}\cdot\boldsymbol{s}=0$), slip rate $\dot{u}$ and fault area A_f, located in a seismogenic volume $V=D\cdot A$ (D = seismogenic thickness, A = map-view area), the moment rate tensor is the double couple:

$$\dot{M}_{ij}=\mu\,\dot{u}\,A_f\left(n_i s_j+n_j s_i\right) \tag{D1}$$

Here $\mu\,\dot{u}\,A_f$ is the scalar moment rate. The term $n_i s_j$ is a force couple with force along $\boldsymbol{s}$ and arm along $\boldsymbol{n}$, and $n_j s_i$ is the perpendicular couple that cancels the net torque.

The strain rate follows from the velocity gradient averaged over V. Slip on the fault is a velocity jump: the velocity changes by $\dot{u}\,\boldsymbol{s}$ across the fault plane and is otherwise uniform. The velocity therefore varies only in the direction normal to the plane, and its gradient $\partial_i v_j$ is zero everywhere except on the fault, where it is a spike with index i along $\boldsymbol{n}$ (the direction of change) and index j along $\boldsymbol{s}$ (the component that changes). The spike integrates across the fault to the velocity jump, so integrating over V leaves the fault area: $\int_V \partial_i v_j\,dV=\dot{u}\,A_f\;n_i s_j$. Dividing by V gives the average velocity gradient, $\dot{u}\,A_f\;n_i s_j/V$, and the strain rate is its symmetric part (1):

$$\dot{\varepsilon}_{ij} = \frac{\dot{u}\, A_f}{2V}\left(n_i s_j + n_j s_i\right) \tag{D2}$$

The factor $\frac{1}{2}$ in (D2) comes from the symmetrization.

(D1) and (D2) contain the same tensor $n_i s_j + n_j s_i$, so dividing one by the other gives the Kostrov (1974) tensor relation:

$$\dot{M}_{ij} = 2\mu V \dot{\varepsilon}_{ij} \tag{D3}$$

The factor of 2 is the ratio between the double couple, which contains both couples, and the strain rate, which contains only their symmetric half. Moment rate tensors and strain rate tensors both add over faults, so (D3) also holds for the sum of many faults within V. (D3) holds for any fault population. It fixes the total moment tensor, not the scalar moments of the individual faults, which depend on the population (D.4, D.5).

D.2. Strike-slip faults: the factor of two cancels

For a vertical strike-slip fault with $\boldsymbol{n} = (1,0)$, $\boldsymbol{s} = (0,1)$, only $\dot{\varepsilon}_{xy} = v\, A_f / 2V$ is nonzero. Since $\dot{\varepsilon}_{xy} = \dot{\varepsilon}_s / 2$ (tensorial vs. engineering shear), the scalar moment rate is:

$$\dot{M}_{ss} = \mu v A_f = 2\mu V \frac{\dot{\varepsilon}_s}{2} = \mu D A\, \dot{\varepsilon}_s \tag{D4}$$

The Kostrov factor of 2 is exactly canceled by the factor of $\frac{1}{2}$ between tensorial and engineering shear.

D.3. Dip-slip faults: the dip correction

For a fault dipping at angle δ from horizontal, two geometric factors enter. The horizontal component of slip is $s\cos\delta$, giving $s = |\dot{\varepsilon}_d| W / \cos\delta$, where W is the width of the area across strike, and the fault area per unit map-view area is $A_f / V = 1/(W \sin\delta)$. The scalar moment rate is:

$$\dot{M}_{ds} = \mu D A f |\dot{\varepsilon}_d| \tag{D5}$$

The dip factor $f = 1/(\sin\delta\cos\delta)$ is symmetric about $\delta = 45°$: both $\delta = 30°$ and $\delta = 60°$ give $4/\sqrt{3} \approx 2.31$, while $\delta = 45°$ gives 2.

D.4. General definition of $\dot{M}_{\text{split}}$

For a partitioned fault system with independent strike-slip and dip-slip populations at dip δ, whose slip does not cancel, the moment rate is the sum of the scalar moments for the strike- and dip-slip faulting (D4+D5):

$$\dot{M}_{\text{split}} = \mu D A \left(\dot{\varepsilon}_s + f |\dot{\varepsilon}_d|\right) \tag{D6}$$

D.5. The minimum moment $\dot{M}_{min}$ of Savage and Simpson (1997)

Savage and Simpson (1997) asked for the smallest moment rate with which faulting can produce a given horizontal strain rate tensor. Their answer is:

$$\dot{M}_{min} = 2\mu\, D\, A \max\left(|\dot{\varepsilon}_1|, |\dot{\varepsilon}_2|, |\dot{\varepsilon}_d|\right) \tag{D7}$$

The third term enters because faulting causes no volume change: the horizontal dilatation requires an equal and opposite vertical strain rate, $\dot{\varepsilon}_3 = -\dot{\varepsilon}_d$ (D.1), and the largest of the three principal values sets the moment. $\dot{M}_{\min}$ is reached when the strain is released by faults on the planes of maximum shear, at 45° to the principal axes. These are vertical strike-slip faults at 45° to the horizontal principal axes and dip-slip faults of 45° dip striking perpendicular to a principal axis. Any other set of faults that produces the same horizontal strain rate tensor, with other orientations or with slip that partly cancels between faults, needs at least as much moment as $\dot{M}_{\min}$, because the moment spent on misoriented or canceling slip adds to the total without adding to the net strain. $\dot{M}_{\min}$ is therefore a lower bound for any fault population, whatever the unobserved vertical shear.

Mathematical argument. For a trace-free moment tensor T, let $N(T)$ be its largest absolute eigenvalue, which is the scalar moment M_0 of a double couple. N is a norm, so for faults whose double-couple tensors T_k sum to T, $\sum M_{0,k} \geq N(T)$. The bound is attained: the convex hull of the double couples with $M_0 = 1$ is the set of trace-free tensors with $N(T) \leq 1$, so T can be built from double couples with total scalar moment $N(T)$. For the strain rate tensor, $T = 2\mu V \dot{\boldsymbol{\varepsilon}}$ has eigenvalues $2\mu V \dot{\varepsilon}_1$, $2\mu V \dot{\varepsilon}_2$ and $\dot{\varepsilon}_3 = -\dot{\varepsilon}_d$, which gives (D7). Removing the unobserved vertical shear components from T cannot increase $N(T)$, so (D7) is a lower bound whatever the vertical shear, and it is reached when the vertical shear is zero. The Frobenius convention for the scalar moment of an individual moment tensor, $M_0 = \sqrt{\mathrm{tr}(T^2)/2}$, coincides with $N(T)$ for a double couple but is smaller for other tensors, by up to 13%, and gives a looser bound.